ATLAS Internal Note
Muon-No-32
16 February 1994

ATLAS MUON DETECTION USING JET CELLS

M. Dris, T. Filippas, E.N. Gazis
Athens NTU

K. Bussmann, J.L. Chevalley, G. Di Tore, C.W. Fabjan, A. Franz, E. Gaumann,
J.Ch. Gayde, B. Goret, W. Klempt, C. Lasseur, J. Raynaud, E. Rosso, G. Viehhauser
CERN

E. Barberio, D. Liguori, M. Schioppa, G. Susinno, M. Valdata-Nappi
Cosenza

A. Balla, H. Bilokon, R. Bonini, V. Chiarella, M. Curatolo, G. Corradi, L. Daniello, B. Esposito,
E. Iacuessa, L. Iannotti, L. Passamonti, V. Russo, M. Santoni, G. Tentori, A. Teodoli, M. Troiani
Frascati

A. Borisov, N. Bozhko, V. Gorjatchev, M. Kirsanov, A. Kozhin, Yu Salomatin,
V. Tumakov, A.S. Vovenko
IHEP Protvino

P. Bagnaia, H. Beker, G. Capradossi, G. Ciapetti, A. Nisati, M. Perciballi, C. Piscitelli,
,L. Pontecorvo
Rome

T. Kobayashi, S. Komamiya, T. Mashimo,
Tokyo

Table of contents

1. Design Concept of the Jet Cell Chamber (JCC)
2. Layout of the Jet Cell Chambers
3. Fabrication of Bi-Cells
4. Support Structures for Bi-Cells
5. Statistical and Systematic Errors
6. Impact of Temperature Gradients
7. Test Results
8. A Comment on Costs

Appendix 1: Parameter List

Appendix 2: A Mechanical Model for the Support Deformation

Appendix 3: Photogrammetry

1. Design Concept of the Jet Cell Chamber (JCC)

The ATLAS muon system will consist of approximately 5000 m2 of high-precision drift-chambers grouped into three layers. The superlayer performance goal is $\sigma_{total} < 70$ μm. The total size of the sensitive surface combined with the required precision demands the application of simple and well-known detection schemes, like drift chambers, preferably working with a saturated drift velocity. A large number of institutes will have to collaborate over many years to construct and operate this big detector. Therefore the fabrication principles and its later operation should aim at utmost simplicity. The design of such a detector should also take into consideration that the ambient temperature in the ATLAS detector will vary in space and in time over several ºC. These temperature differences will be difficult to control. Consequently, a technology intrinsically stable under temperature fluctuations should be considered. In addition to the precision drift chambers, approximately 10 000 m^2 of trigger-planes will be needed; they are, however, not discussed any further in this note.

The Jet Cell concept features a highly modular approach. The detector is subdivided into 512 modules with sizes up to 3 x 8 m^2. Each module consists of a simple support structure, made of sandwich carbon fibre plates, and approximately 25 double drift cells, so called bi-cells. Carbon fibre has been chosen for its thermal stability. The bi-cells are mounted on top of the support structure to form the sensitive layer. Each bi-cell is inclined by 20.7^0 to an infinite momentum track from the interaction point. The layout of a bi-cell is schematically shown in Fig. 1. It consists of 2 separated drift cells each equipped with 6 to 8 sense wires, 30 to 40 μm thick, and 12 to 14 field wires with a diameter 100 to 150 μm. The wires are divided into two groups in each cell. In this way each track will cross two different drift regions. Thus auto-calibration and T_0 determination can be performed. The bi-cells are closed with aluminium covers. The two cells of a bi-cell are separated by an aluminium sheet. If the 2nd coordinate is to be measured, this sheet could be replaced by a printed circuit board to provide strip read out.

The Jet Cell with its well-defined drift geometry uses a 'fast' drift gas (e.g. $N_2/CO_2/CF_4/CH_4$) in saturation. We have refrained from using 'slow', non-saturated gases for the following reasons:

– we wish to keep the maximum drift time to below ~ 500 ns;

– slow, non-saturated gases are typically an order of magnitude more sensitive to temperature, pressure and mixture variations compared to fast, saturated gases.

The total measurement error, σ_{total}, is composed of many contributions and will be discussed in detail in Section 5. All of these errors will have to be controlled carefully; however, special attention has to be given to SYSTEMATIC errors which may increase as the system is scaled from prototype dimensions (≤ 10 m^2) to the final size. This implies the need for a design concept which will provide the SAME resolution in the final detector as for test beam prototypes. This is a requirement so rigorous that it has rarely -if ever- been achieved in large systems.

A further concern is the stability of operation of such a large system. The ATLAS system will be the largest particle physics detector ever built and it will operate in one of the most hostile environments for such a detector. An appropriate level of prudence and conservatism must be exercised to provide certain 'safety margins' in the operation to achieve the desired level of performance in the complete system.

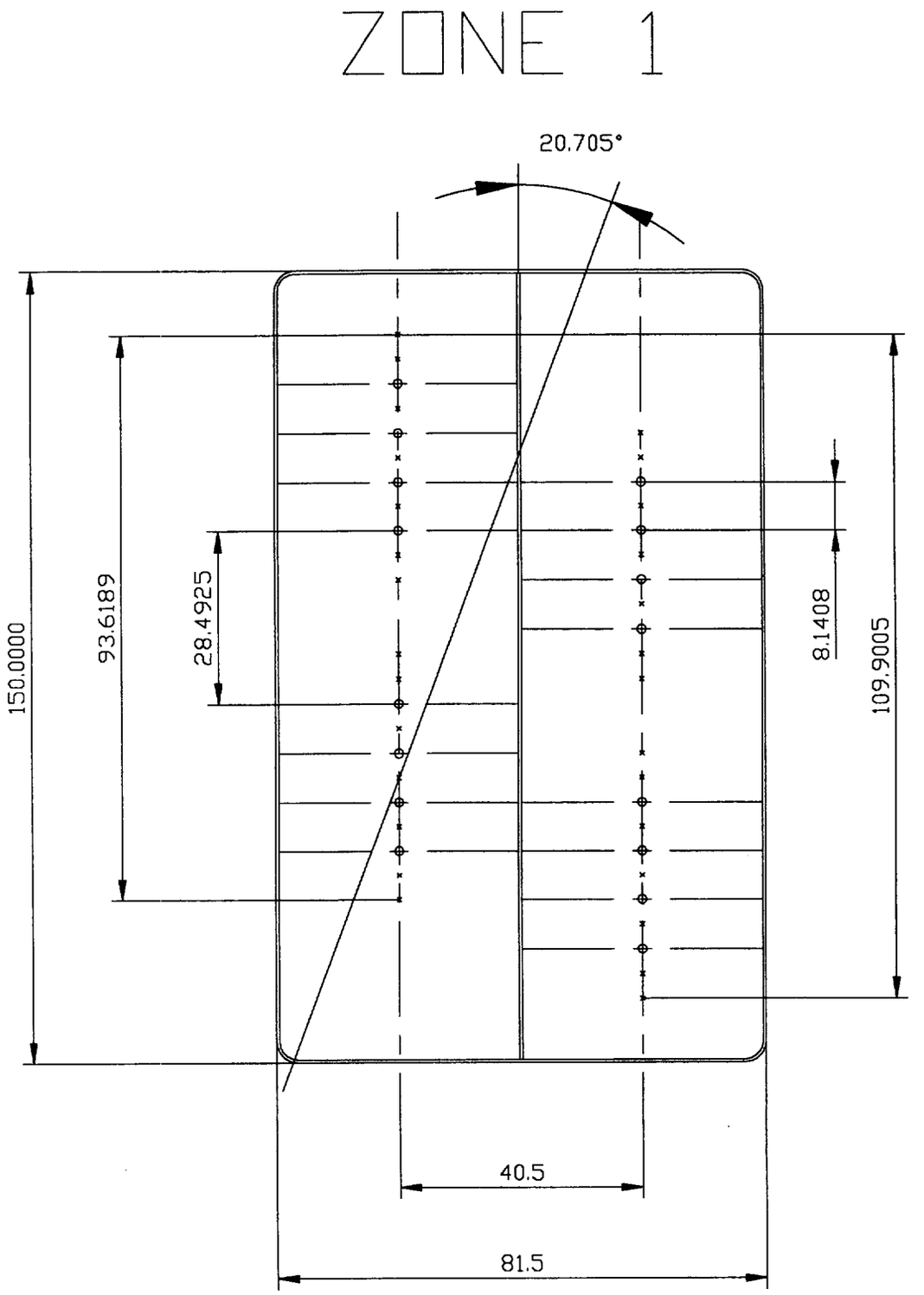

Figure 1
Layout of a bi-cell. The crosses indicate field wires and the open circles show the sense wires (dimensions are in millimetres).

This note develops and documents in detail the arguments in favour of the JCC technology :

i. All the wires which are statistically combined to provide a precision point, are located in the same (or in neighbouring) gas enclosure(s). This arrangement is optimally suited to reduce systematic errors at the 'local' cell level.

ii. The Jet Cell has very high local geometrical acceptance and uses a uniform drift operation. Reconstruction of local track vectors is therefore robust, particularly in view of its demonstrated good multi-track capability.

iii. The local accuracy, as a result of the achievable statistical and systematic errors, can be characterised by ONE parameter (bi-cell location tolerance), in common for all 12 or 16 wires in a bi-cell. This will be useful when ultimate control of systematic errors will be attempted, i.e. using particle tracks.

iv. Global control of systematic errors requires only ONE further step: location of the modular bi-cells on a precision support. The locating holes will be drilled under computer-control relative to the external alignment fiducials. The only requirement is a precision drill with adequate working surface ($\leq 3 \times 8$ m^2). Such machines are quite readily available (they could even be rented and located on the premises of an institute) and provide access to the simplest mechanical precision operation, i.e. drilling. Construction of these supports from C-fibre material would guarantee long-term stability in a possibly adverse thermal environment.

v. The JCC technology lends itself naturally to final system checks – using photogrammetry. This information can be used at the start-up of ATLAS to further correct the already small mechanical tolerances to a level at which they will no longer have any impact on the spectrometer resolution.

Jet Cell drift chambers are the most widely used technology for precision trackers. The extension to the 'Tilted Jet Cell' (CDF, H1) has led to very powerful detectors in which 'auto calibration' has been shown to control drift chamber errors.

In summary, the Jet Cell design concept, as presented here, is based on the principle to assemble the total detector in a simple way with relatively small and simple pieces. For the fabrication of the support structures we foresee a simple assembly from rectangular carbon fibre sandwich plates delivered in the right sizes by industry. The only manufacturing requirement is a precision drilling machine with a working surface of the size of the structure. The bi-cells are made of a kit of relatively small and precise items (length ≤ 1 m). The assembly technique has proven to be easily transferable to collaborating institutes: prototypes have already been successfully produced at CERN and Frascati.

2. Layout of the Jet Cell Chambers

The proposed layout for the barrel region of ATLAS is shown in Fig. 2. Indicated are the three superlayers positioned at three different radii of the ATLAS toroid.

As shown in the figure, the support structures are on both sides approximately 40 cm shorter than the bi-cells. This allows a compact arrangement of the layout. The outer layer is made

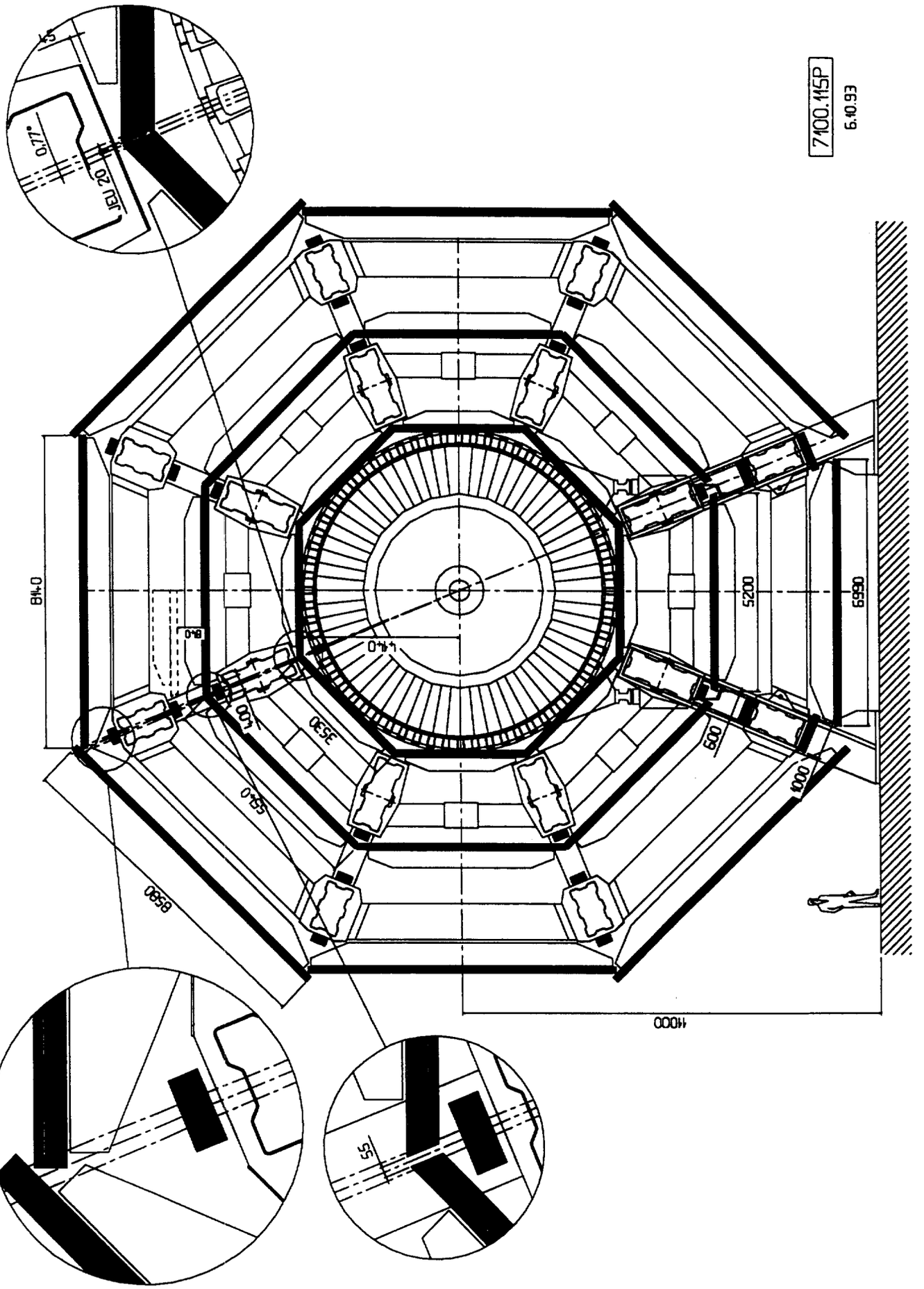

Figure 2
Proposed layout of the barrel region using the Jet Cell technology
(dimensions are in centimetres).

of chambers with different lengths (8.1 m and 8.6m) in the ϕ-direction in order to provide an overlap between neighbouring modules. The middle and inside layers, with lengths of 5.5 m and 3.5 m respectively, cannot be made to overlap for geometrical reasons.

In the z-direction the chambers have widths varying from 1.8 to 3 m. The widths have been chosen in such a way that towers can be established in which all modules are aligned by four alignment rays in the corners to correct the sagitta measurements for displacements of the modules. The clearance between two adjacent modules is ~ 20 mm. This will not, however, introduce dead zones since the bi-cells are inclined by 20.7° with respect to straight tracks.

The inside layer has a clearance of 20 mm between the chambers in the ϕ-direction. Assuming conservatively a dead zone of 20 mm at the ends of the bi-cells, one estimates a loss of <1.5% of the total area in the barrel zone. The chambers of the middle layer have a clearance of approximately 55 mm. The corresponding dead zone will be completely covered by 128 chambers with a wire length of 0.6 m and widths of 1 to 2 m. As indicated in Figs. 2 and 3, these chambers will also cover the dead regions caused by the struts in the magnet.

A conceptual layout of the end caps is shown in Fig. 3. The support structures have a trapezoidal form and the length of the bi-cells varies along the module.

All the bi-cells are inclined by 20.7° with respect to a straight track from the vertex. Each track will be measured by at least 5 sense wires in each superlayer. As a result the wire layout of the bi-cells has to vary with respect to the angle between a straight track and a module. We foresee 4 different zones. For impact angles from 0° (perpendicular to the module) to 6°, there will be 8 sense wires in a cell, for the range of 6° to 17°, seven sense wires. For the rest we have two different layouts of cells with 6 sense wires each. The wire layout of the bi-cells for the different zones are shown in Fig. 4. This layout minimizes the number of readout channels. Final optimization may favour a slight increase in this number.

It should be noted that in the 'optimised' layout there is complete coverage with three measurement planes, with the following exceptions:

– in the shadow of six coils there is an angular region of 6 x 0.77^0, where in the present layout only two measurement stations are planned; this represents 1.3% of the complete azimuthal coverage. This region should be instrumented with chambers providing an angle-angle measurement;

– in the shadow of the support feet (~ 4% of the azimuth) special chamber arrangements are required for all three technologies; we plan to use a layout again allowing an angle-angle measurement, similar to the concept shown in the LOI.

3 Fabrication of Bi-Cells

The sensitive area of the ATLAS muon detector will be covered by approximately 12000 bi-cells. The field and sense wires will be stretched over the total length of the bi-cells varying from 1 to 8.6 m. They have to be supported about every metre to minimise the gravitational sagitta. Fig. 5 shows a schematic drawing of a bi-cell with an intermediate length of approximately 4 m. On each end, precision injected moulded plastic pieces will hold the field and sense wires of the 2 bi-cells. Every 1 m a support piece, also made of injected moulded plastic, will keep the wires in position. Covers made of aluminium will close the bi-tube. As can be seen in Fig. 5 the

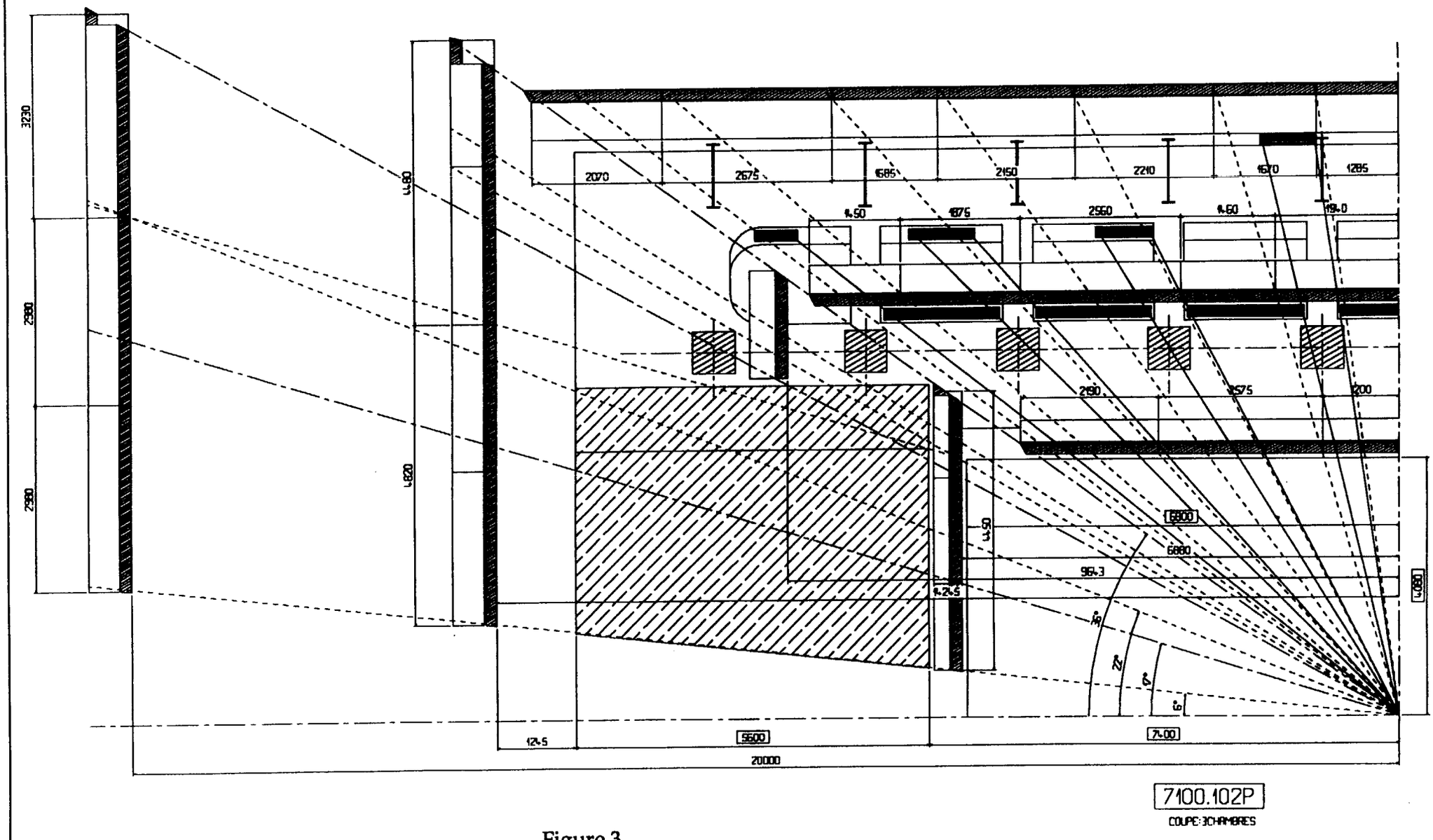

Figure 3
Conceptual layout of the ATLAS endcaps using the Jet Cell technology
(dimensions are in centimetres).

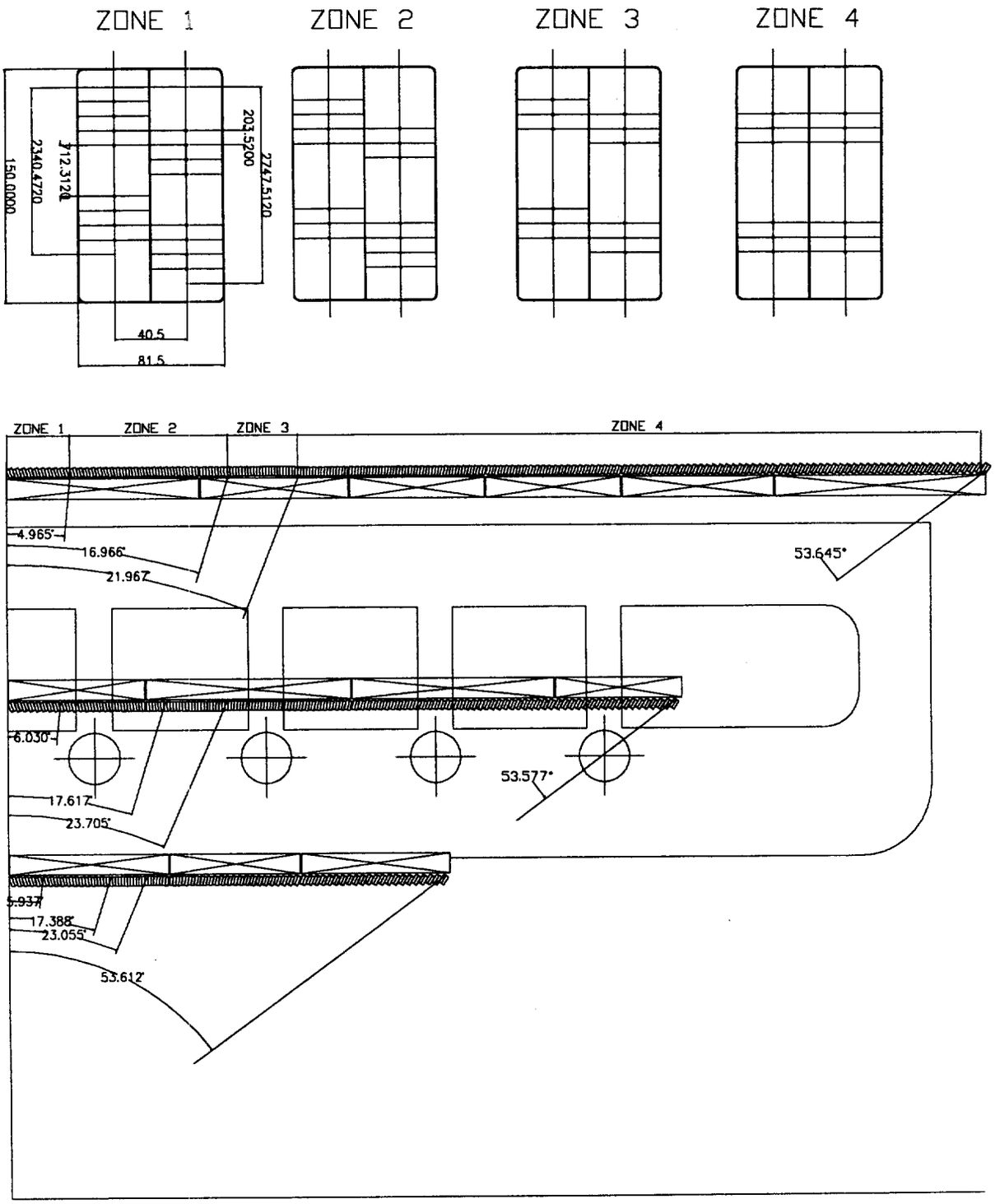

Figure 4
Layout of the Jet Cell wires for the four different zones in polar angle.

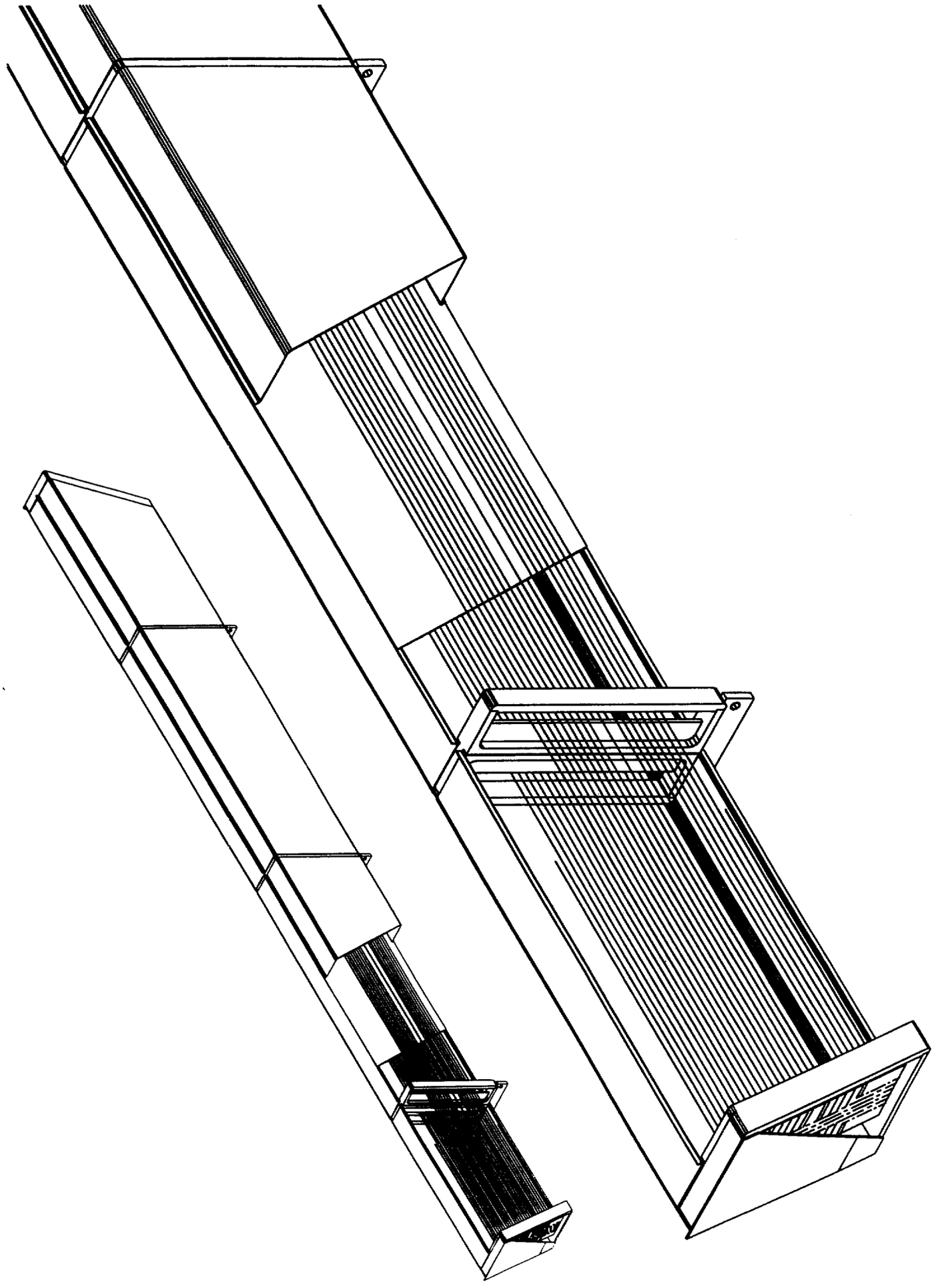

Figure 5
Schematic drawing of a bi-cell of 4 m length, corresponding to the design used for the prototype.

intermediate wire support frames will be open to one side during wiring and later closed by a plastic piece to allow the closure with the covers. The end pieces will also be open for wiring. As indicated in Fig. 6, they will include Cu-Te support blocks in which the wires will be crimped. These blocks will be connected to a printed circuit board and glued to the end pieces. If the crimping blocks cannot be positioned precisely enough, precision combs will be integrated into the moulded end piece.

For the mass production, we foresee seven assembly benches to produce such tubes. These benches will support the wire frames of a bi-cell at their nomimal position with an accuracy of less than 20 μm. The seven benches will serve, as indicated in Fig. 7, to build all the bi-tubes with lengths varying from 1 to 9 m. We foresee the following steps for the bi-cell production:

1) The open end pieces and the intermediate wire supports will be attached to the fixations on the bench.

2) The fixations are then rotated about the cell axis to position the supports horizontally (for wiring). With a wiring machine we will be able to wire at the same time one half of a cell or 9 to 11 wires. For this purpose the wiring machine (Fig. 8) will be placed horizontally in the correct position with respect to the support frames. Subsequently, the wires will be crimped in their corresponding Cu-Te blocks and the wires will be stretched over the whole length of the tube. At the other end the wires will be stretched by applying the appropriate weights to ≤ 30 % of their elastic limit. The tension will be chosen in such a way that the gravitational wire sag will be identical for wires of different diameter. After stretching, the wires will be crimped into the Cu-Te blocks and cut. The wires are then glued to the intermediate supports. After completion of one side of the bi-cell, the supports are rotated by 180° and the second cell is wired.

3) Once the wires are stretched and crimped, the supports will be put into the vertical position, where, first, the closures of the wire supports are glued. The central aluminium walls are put into position and the aluminium covers are glued to the tube.

   We estimate that every day on each bench one bi-tube with lengths from 4.5m to 9m or two bi-tubes with lengths below 4.5m will be assembled.

4) Once the bi-tubes are fabricated, they will be individually tested for leak tightness and correct electrostatic behaviour.

5) After the acceptance test, the tubes will be equipped with readout electronics and mounted onto the carbon fibre support structure. The gas and electrical connections will also be made. We foresee two mounting stands. One will be just to equip a supermodule, while the other one will serve as a test stand for the final acceptance test.

6) As a last step, the position of all the wire frames will be measured relative to the alignment marks by photogrammetry as described in Appendix 3. For this purpose, all the end frames and intermediate wire supports will be equipped with 2 reference marks. Experience has shown that such a measurement can be done in typically 2-3 hours. The measurement will be made with the supermodule inclined in the same position as it will be later installed in the ATLAS detector. This provides the possibility to enter the actual frame positions into the data base for possible offline corrections.

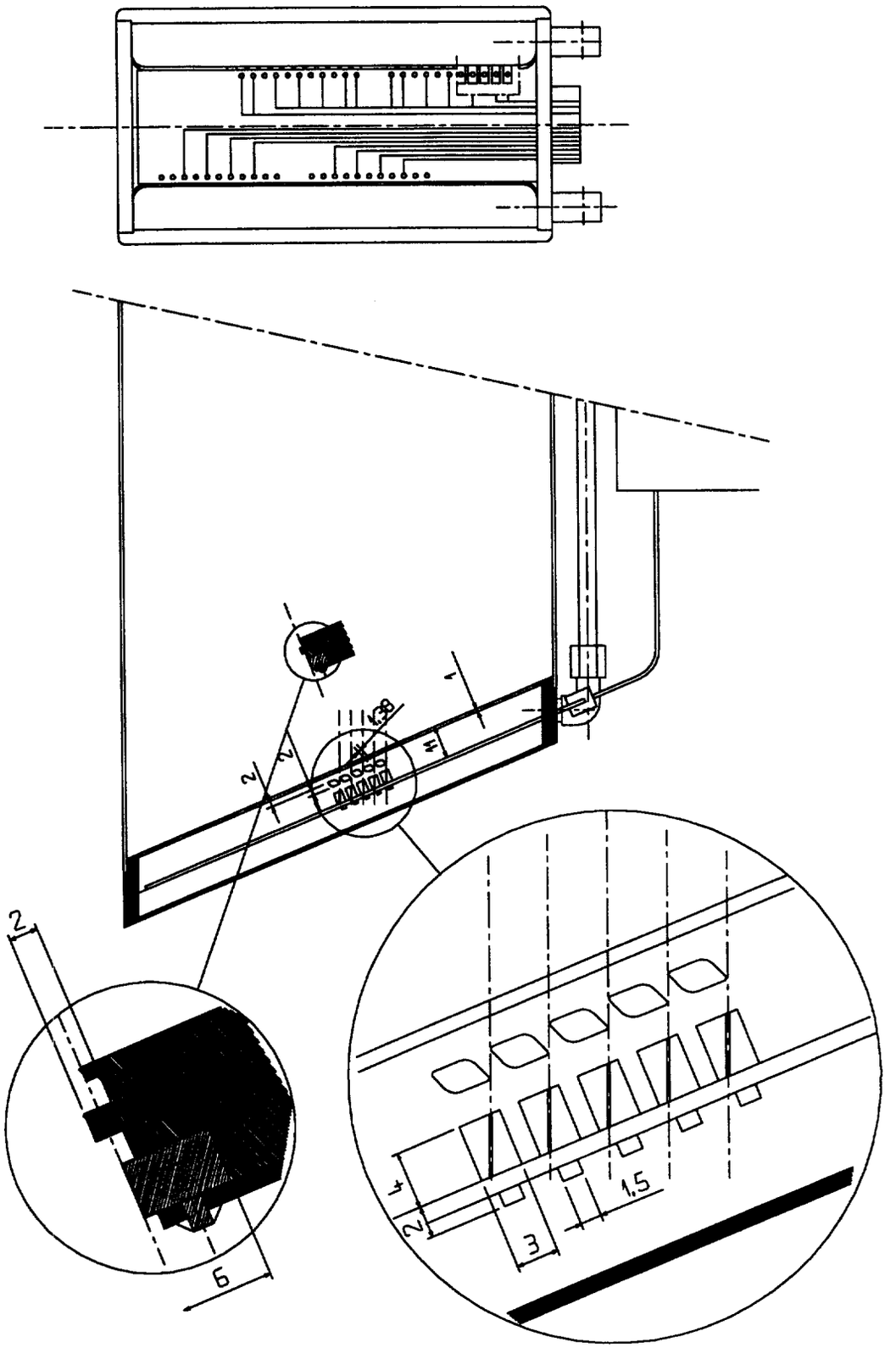

Figure 6
Details of the end frames. Cu-Te blocks will be used to crimp the sense and field wires. A printed circuit board provides the electrical connection between the Cu-Te blocks and the preamplifiers.

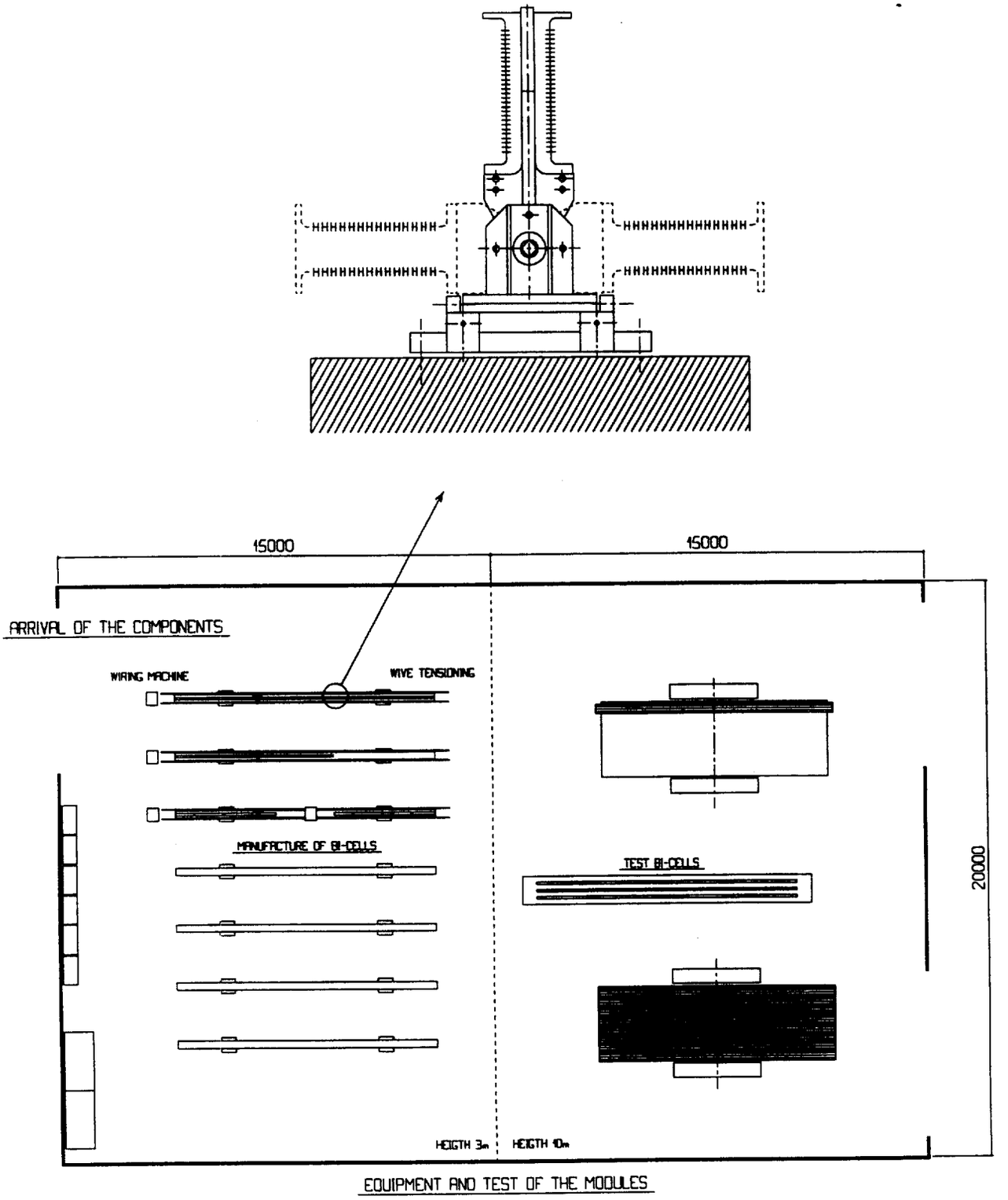

Figure 7
Layout of the assembly area indicating the seven precision benches on which the various frames will be positioned. Also shown is an enlarged view of the cross-section of such a bench indicating the three different positions for the wires frames during bi-cell production.

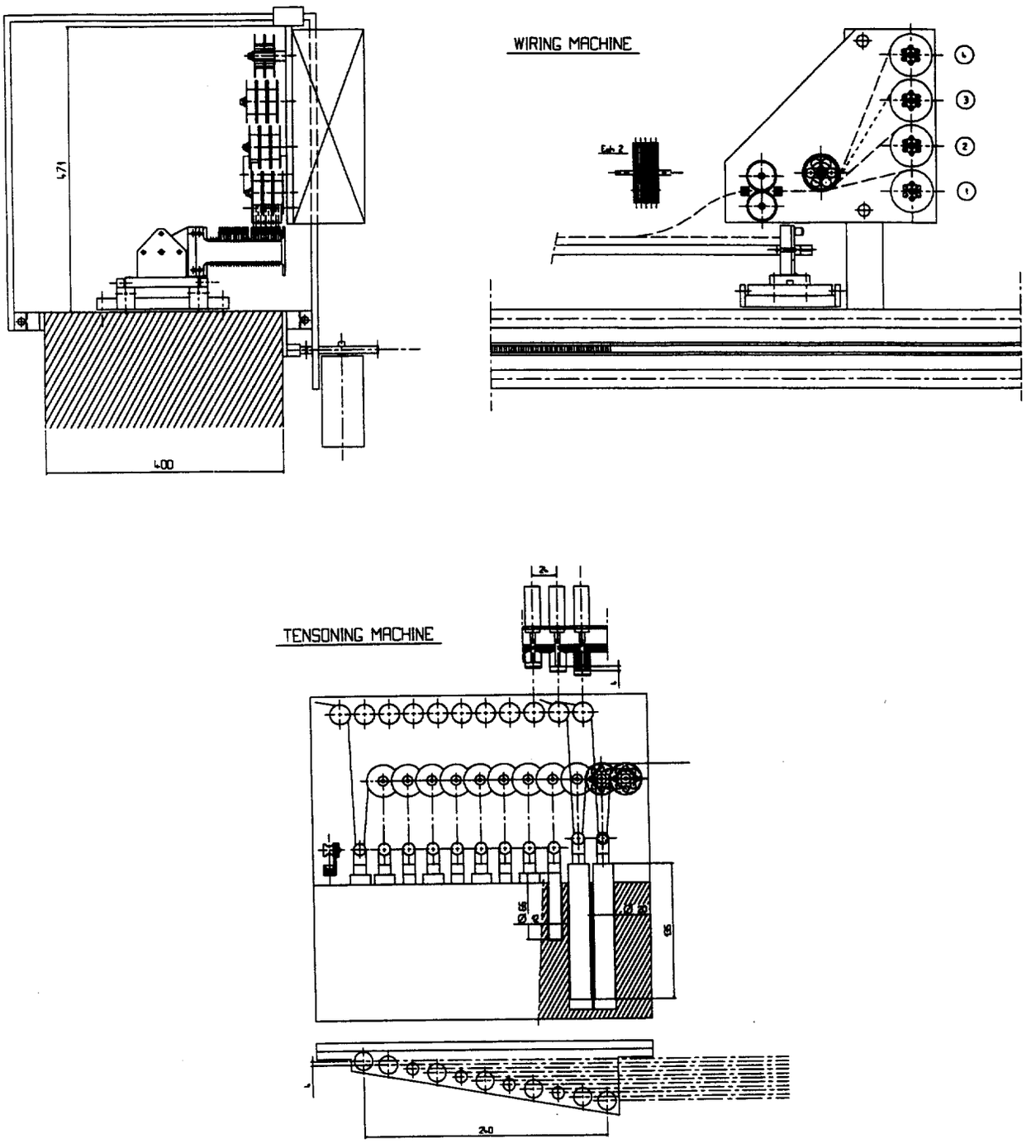

Figure 8
Three views of the wiring machine used for the wiring of the Jet Cell. Half of all the wires (9 to 11) will be strung in one operation.

The finished module will be stored awaiting installation into the ATLAS detector. The production rate will be 2 modules per week in order to finish the total detector within 5 years. Since we envisage an installation time of 1 year, the production of 4 years will have to be stored.

4. Support Structures for Bi-Cells

A technical design of the support structure is shown in Fig. 9. As an example we have chosen a structure of the outer layer of the barrel with a length of 8.24 m, a width of 2.67 m, and a height of 0.6 m.

The module is glued together from rectangular composite material sandwich plates. The two skins are made from unidirectional carbon fibre mats, each 1.2 mm thick. The core material is an aluminium honeycomb structure, 25.4 mm thick. The total thickness of the plate is 27.8 mm. The module gets its stiffness from 12 vertical plates, 3 running in the length direction and 9 running in width direction. The module is closed by the top and bottom plates to form rigid I-profiles together with the corresponding vertical plates. In this way, a very stable but light structure is obtained.

To mount the 31 bi-tubes onto this module 9 rows of brackets are incorporated in the top plates running in the width direction. After the structure has been assembled to a moderate precision of $\pm$ 2 mm, holes are drilled into the brackets using a drilling machine with a working surface of the dimensions of the module. These holes define the position of the bi-cells relative to the alignment references and are drilled with a precision of $\pm$ 30 μm (2σ tolerance). At the same time and with the same precision fixation holes for the alignment system will be made. It should be noted that only a relative precision of all these holes is required and therefore this step in the manufacture is relatively simple.

The weight of the support structure is approximately 190 kg, the weight fully equipped is 442 kg. Finite-element calculations have shown that the total deformation of the complete structure including bi-tubes will be 128 μm for the horizontal modules and 16 μm for the vertical ones. This implies a unit weight of ~20 kg/m^2 and $0.04X_0$ radiation lengths in thickness.

A prototype with dimensions of 4.3 m x 1.7 m x 0.6 m has been manufactured in industry using the above mentioned technique. Control of mechanical precision and the static deformation under load have been in complete agreement with the specifications and the finite element calculations.

The modules are supported in the experiment by 4 support points in a way that no stresses can be transmitted via the support to the structure. It is intended to mount the modules of one sector onto two rails running along the z-axis of the experiment. The rails will be positioned to a precision of $\pm$ 5 mm over the full length of the detector of approximately 26 m and fixed to the magnet cryostat. Therefore the support feet will have to accept the misalignment and the movements of the cryostat during cooling down in a way that no stress is transmitted to the support structure. In Fig. 10 a conceptual design of the proposed support feet is shown. As indicated, seven independent articulations (7 rotations and 4 translations) are needed to achieve the design goal. Fig. 11 shows how this mechanical system can be integrated into the support structure without using additional space.

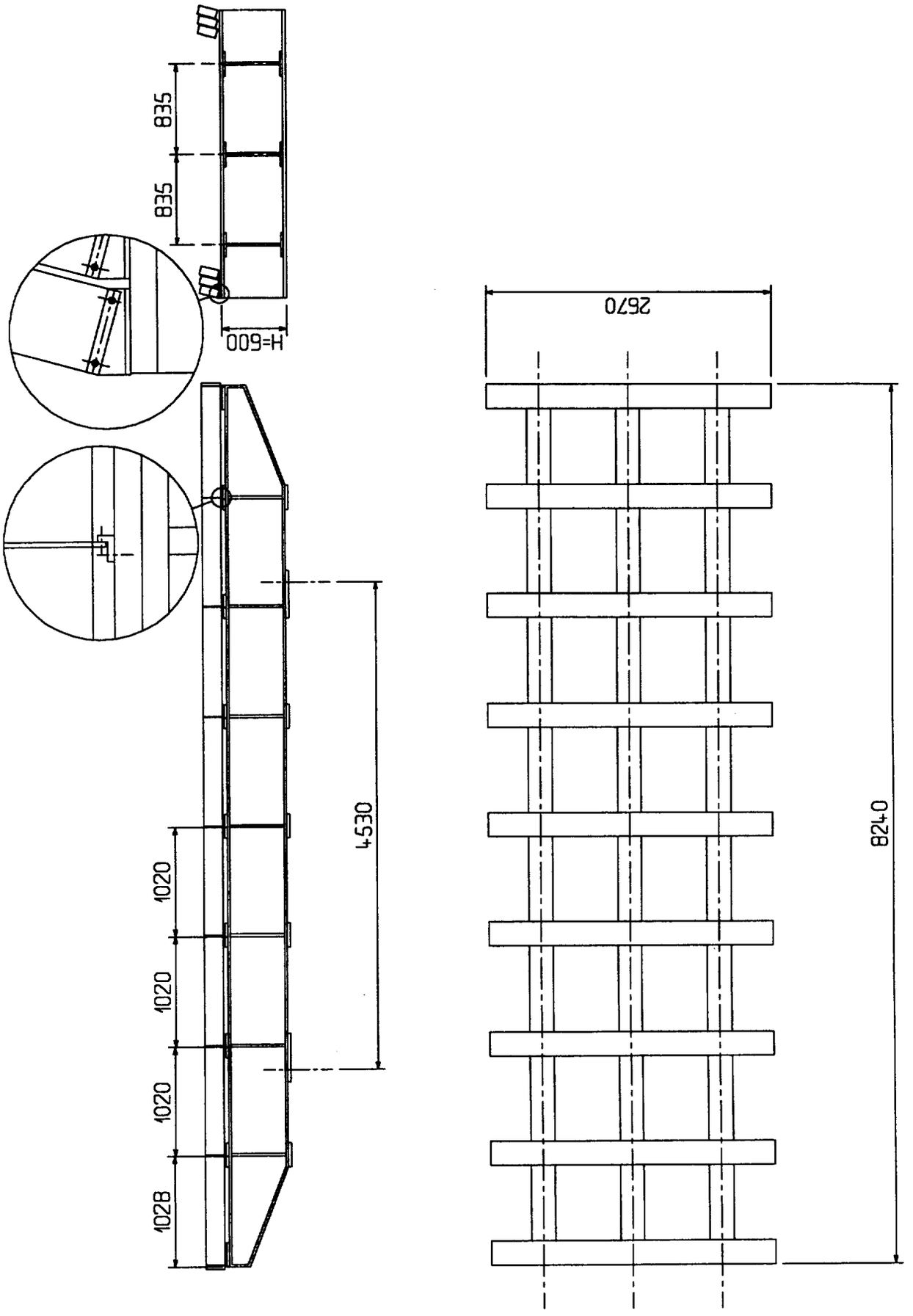

Figure 9
Drawing of the support structure. The dimensions correspond to super modules in the outermost layer of the barrel. (Dimensions are in millimetres).

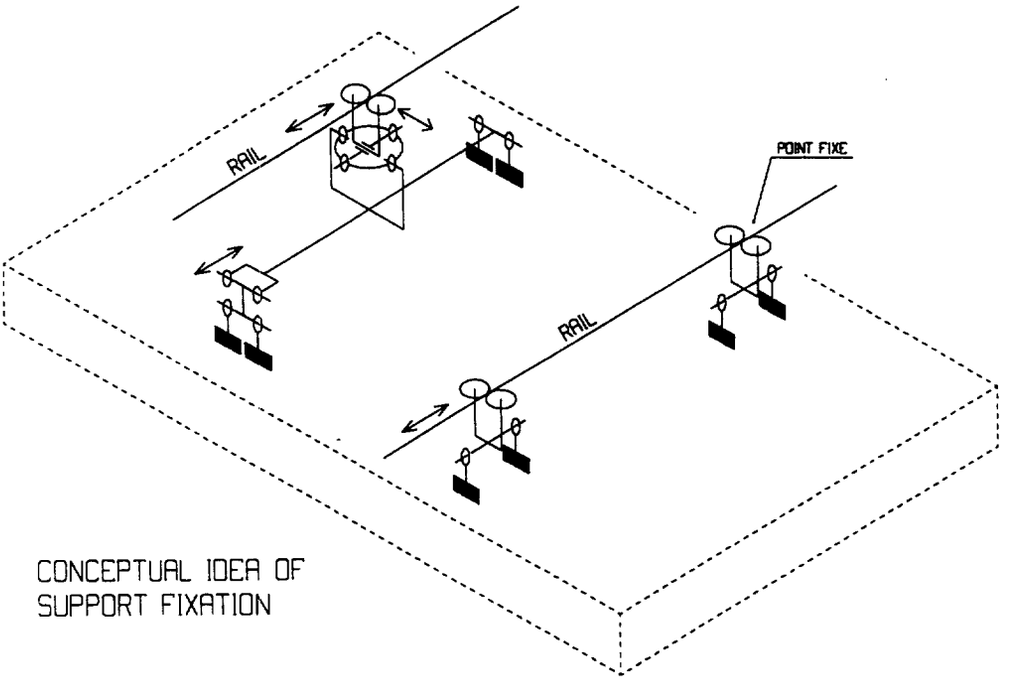

Figure 10
Conceptual design of the feet supporting a supermodule.

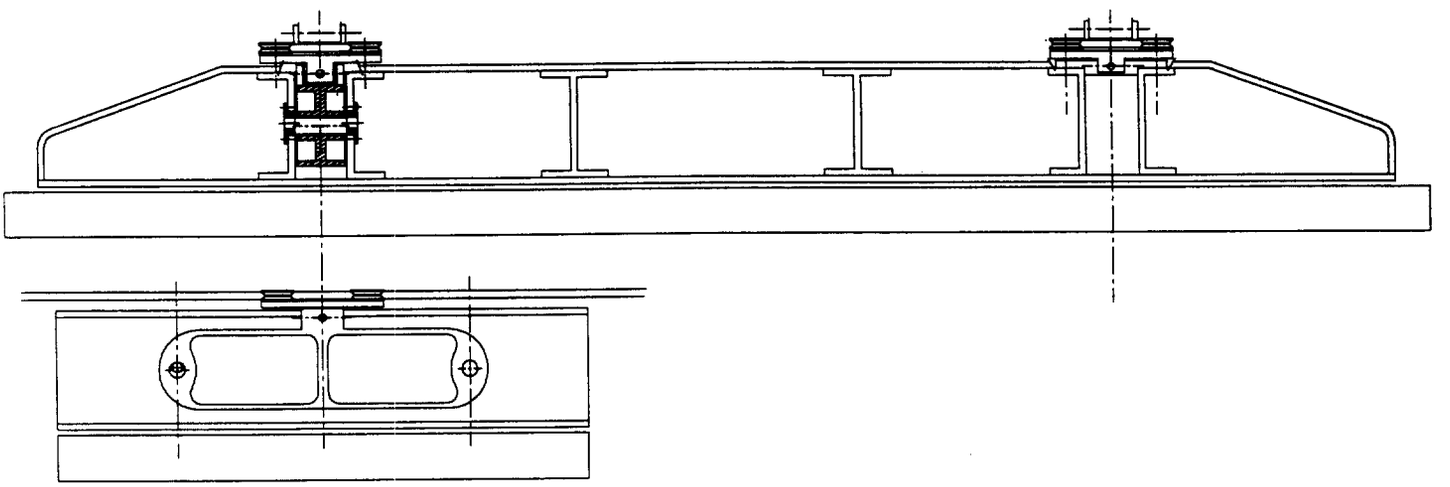

Figure 11
Integration of the support feet into the support structure.

5. Statistical and Systematic Errors

In this section we list, discuss and quantify tolerances and errors which limit the achievable accuracy of the sagitta measurement.

5.1 Wire positioning

The wires will be held in metallic inserts (e.g. Cu/Te blocks) which in turn are positioned in injection-moulded flanges (at the ends) and frames. Tolerances with respect to alignment marks and flange locating holes, are estimated, following discussions with industry, as:

Tolerances [t]	**r.m.s equivalent error**
wire in metal insert t = 20 μm	σ = 10 μm
metal inserts w.r.t. flange locating holes t = 10 μm	σ = 5 μm
wire w.r.t. flange locating holes:	$\sigma_{\text{wire pos.}}$ = 11 μm

These mechanical wire position errors will be amplified by electrostatic forces [1, 2]. These effects arise due to the differences in the wire sag between the sense and potential wires, caused by small (<10%) variations in the nominal wire tensions. The wire positioning error is amplified by a factor F, which is calculated for our geometry and operating conditions to have the value F = 1.5. Consequently, we assign a global wire position error, including electrostatic effects, of

$$\sigma_{\text{wire pos.}} = 17\ \mu\text{m}$$

5.2 Gravitational Wire Sag

Wire sagging contributes to the wire position error. The gravitational sag is limited through construction to a maximum of σ = 40 μm. This is achieved by supporting the wires approximately every metre. The wires (Cu/Be of ~ 40 and ~ 120 μm diameter) are tensioned at < 30% of their elastic limit. This tension is considerably lower than the wire tension employed in most drift chamber systems, where usually a tension of 80% of elastic limit is applied and considered to be safe. Our limit of < 30% is chosen with the aim to reduce the probability of wire breakage by an order of magnitude compared to the most reliable present systems.

Analysis of this problem provides the following results:

maximum gravitational sag (measured)	s = 40 μm
average sag	$\langle s \rangle \approx 2\ s/3$
equivalent gaussian error	$\sigma \approx s/3$ = 13μm

Next we consider the impact of the wire displacement error on the sagitta measurement. The effect is rather similar to the error to the non-planarity of supports (see point 5.5) and is treated in the same way. This Gaussian error of 13 μm will result in a contribution to the superlayer error after averaging over ϕ and θ (see section 5.5 and Appendix 2) of

$$\langle \sigma_{\text{wire}} \text{ displ.} \rangle = 0.24 * 13\ \mu\text{m} = 3\ \mu\text{m}.$$

5.3 Bi-cell positioning

The bi-cells are doweled into precision-drilled holes of support brackets on the super-module support. Based on the experience with the prototype [3] (Section 4) we consider conservatively the already achieved precision as the tolerance for the absolute location of the bi-cells relative to external alignment references (e.g. Rasnik). The angular positioning and its error are governed by a second tolerance on the relative location of the two holes/frame for the dowel pins. This relative alignment error contributes to an angular positioning error, amplified by the ratio of the (average) height of the cell (<H> = 9 cm) relative to base width of the cell support which is 5.5 cm. We arrive at the following tolerances and the equivalent r.m.s. errors:

Tolerances	**r.m.s equivalent error**
fixation holes relative to external alignment (achieved in prototype) t = 30 μm	σ = 15 μm
relative positioning of the two fixation holes with t = 10 μm (σ = 5 mm) gives equivalent positioning error	σ = 8 μm
total error of cell positioning relative to external alignment	$\sigma_{\text{bi-cell pos}}$ = 17 μm

5.4 Mechanical Deformations Causing E-field and υ_D Variations

In the JCC the wires are located in space with very high precision, as discussed previously. The cathodes will be made of very thin metallic foils (e.g. 0.3 mm thick aluminium sheets).

Although these foils are supported by frames and spacers at regular intervals (typically every metre) certain deformations will have to be accepted. Based on our prototype work, we assign a tolerance t to the flatness of the cathodes:

t (cathode flatness)	= 0.6 mm;
r.m.s (cathode flatness)	= 0.3 mm;
r.m.s. (E_D-field)	= (0.3/20) * 2.0 kV/cm
	= 0.03 kV/cm

These variations in the drift field will induce local drift velocity variations if the drift velocity is not highly saturated.

While we have not finalised the choice of the drift gas, we have candidate mixtures ($He/CO_2/CF_4/C_4H_{10}$ or $N_2/CO_2/CF_4/CH_4$, see Appendix 1), for which a good saturation

$$\frac{\Delta v_D}{\Delta E} \leq 0.04 \text{ cm}^2 / \mu\text{s kV};$$

and a low Lorentz angle of $\theta_L < 12^\circ$ at B = 0.9T at low drift fields E_D < 2.0 KV/cm was calculated.

Based on these measurements and assumptions, we arrive at an error to the position measurement due to local E_D-variations:

$$\sigma (E_D - V_D) = 3 \mu\text{m}.$$

5.5 Deformation of Support

We have analysed the mechanical model of our support and the contributions to the sagitta error caused by the deformation of the support. In particular, the support of the outermost chamber, which may have to span close to 8 m, will be constructed from C-fibre panels, such that it will sag by a well-defined amount; we know that, for practical constructions, this sag S will be $S < 0.15$ mm in the 'long' direction, i.e. in the ϕ-direction. Note also that due to the kinematical support in the optimum position (approximately 0.22 * length away from the edges) the edges will also sag by the same amount of S. (Appendix 2).

A summary of the full calculation, carried out for somewhat different assumptions, is attached (Appendix 2). Here, we quote the results which were obtained under the following assumptions:

- sag of each support (inner, middle, outer layer) by $S = 0.15$ mm;
- error on the sag assumed: $\sigma = 30$ μm. Note that this error is comparable to the one measured on the prototype, using photogrammetry (σ deformation, measured ~ 30 μm).
- averaging over $36^\circ < \theta < 90^\circ$
  over $0^\circ < \phi < 360^\circ$

Under these assumptions, we find a contribution to the sagitta error of one superlayer σ (deformation) = 8 μm.

5.6 Errors due to Temperature Variations

Two effects are of concern:

a) temperature-induced dimensional changes of the chambers (+ supports), assuming uniform temperature ($\Delta T < 0.1^\circ$ K) of a super-module;
b) temperature gradients across and along a super-module.

We expect that dimensional variations due to the first effect can be corrected by our projective alignment system. Such dimensional changes are of the order of 120 μm/metre for a temperature change of $\Delta t = 5^\circ$ K in the case of an aluminium structure; it is approximately a factor of 25 smaller if carbon fibre sandwich structures are used to control the dimensional stability.

The second effect is potentially much more dangerous (see section 6). For example, it has been estimated that a temperature gradient of $\Delta T \leq 1^\circ$ K across a 60 cm support structure could induce deformations of approximately 100 μm on a typically 8 m long structure built from aluminium [4]. Given the rather confined nature of ATLAS, the closeness to different instruments (calorimeter, toroid coils) and the inevitable electronics and power supplies, we could easily be confronted with temperature gradients of order $\Delta T \approx 5^\circ$ K.

Using this estimate, we arrive at a possible deformation for our C-fibre supported detector modules d ($\Delta T = 5^\circ$ K) = 20 μm.

Such deformations will contribute to the superlayer error in a similar way as the support deformations (Section 5.5). We attribute the following error to it:

$$\Sigma\ (\Delta T = 5^\circ\ \text{K}) = 5\ \mu\text{m}$$

5.7 Summary on Tolerances

In this Section, the various tolerances, contributing to the measurement error, are combined such that the measurement accuracy per superlayer is obtained.

Stochastic errors:

σ_{drift} (average over drift cell) = 120 μm [All measurements presented in Section 7]

$\sigma_{wire\ pos.}$ = 17 μm [measured]

$$\sigma_{6w}^2 = (\sigma_{drift}^2 + \sigma_{wire}^2)/6 = (49\ \mu m)^2$$

The full error of a 'cell' requires the addition of bi-tube positioning error $\sigma_{bi\text{-}cell,\ pos}$

$$\sigma_{cell}^2 = \sigma_{6w}^2 + \sigma_{bi\text{-}cell,\ pos}^2 = (52\ \mu m)^2$$

Systematic errors:

The systematic errors quoted here are averaged over the full barrel acceptance.

σ(deformation) = 8 μm [measured: 8 μm]

σ(temperature) = 5 μm [estimated, assuming ΔT = 5 °C]

σ(alignment = 30 μm [assumed]

Finally, after quadratic combination of all errors, the measurement accuracy of a superlayer is found to be:

$\sigma_{superlayer}$ (all errors) = 61 μm, (including 30 μm alignment error)

Please note that in this analysis, the essential errors quoted are based on measurements. The error to the sagitta measurement would be further reduced if alignment with particles is considered. Such an alignment would appear relatively straightforward, as it would be enough to obtain one parameter per bi-cell (position relative to alignment references). We estimate that such a procedure may result in a $\sigma \lesssim 55$ μm error.

A further very effective way to substantially reduce (i.e. by approximately 15%) the sagitta error is to increase the number of measurements in the sagitta plane from 6 to 12 measurements.

6. Impact of Temperature Gradients

All the calculations have been carried out using the finite element program COSMOS 1.65. In Fig. 12 the model used is presented. Two skins with a length of 8.2m of either aluminium or unidirectional carbon fibres are separated by 600 mm of aluminium honey comb material. For the temperature studies we used a two-dimensional model, with the structure supported on the bottom skin by two points. The position of these points was chosen in a way to minimize the deflections under gravitational load. The top skin supports the bi-cells on 9 points, the first of which is blocked and the others allow a free movement in longitudinal direction. It should be noted that in this way no additional stress due to thermal expansion is added to the support structure and the bi-cells will not contribute to the mechanical stiffness of the structure. Additionally, the air space in the 30 mm

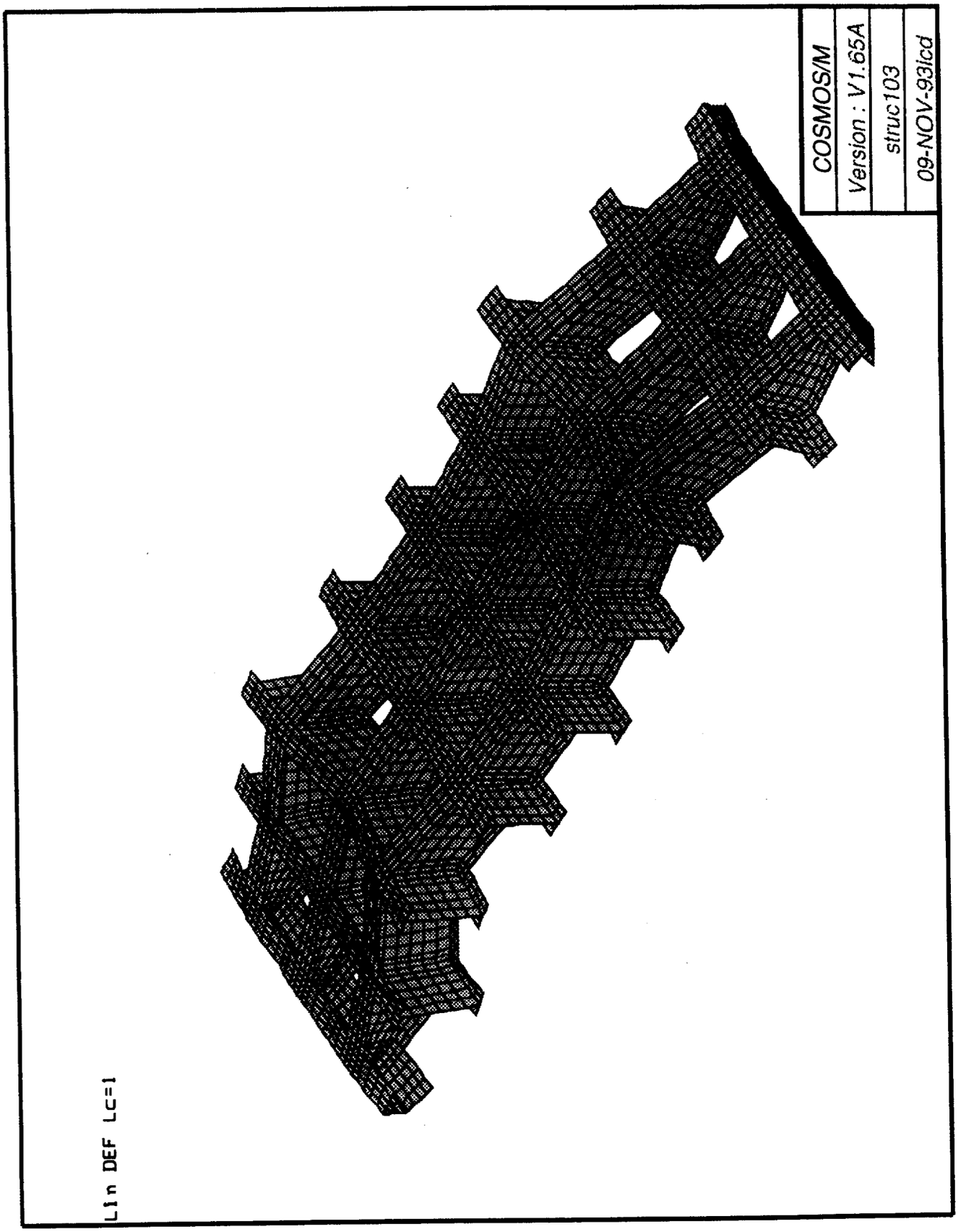

Figure 12
Model used for the finite-element calculations for mechanical and temperature deformations. Shown are the maximum deformations of a 8.2 m long structure in the horizontal position (sag = 128 μm).

gap between the cell structure and the bi-cell had to be modelled since it has an important influence on the heat transfer through the structure.

The thermal load has been assumed to be a difference in the air temperature of 1°C outside the top and bottom layer of the respective structures using a heat transfer coefficient between the surrounding air and the structure of $\Lambda = 5.53$ W/m^2 °C. We consider this assumed temperature difference very small and difficult to obtain in a closed environment like the ATLAS detector. One may obtain realistic values by multiplying the following results with a more realistic temperature difference.

Table 1: JCC monoblock structure with various materials under thermal load.
An air temperature difference of 1°C has been assumed.

Skin	Honey comb	Sag (μm/°C) due to air temp. diff.
Aluminium	ACG 3/8-0.003	46
Aluminium	ACG 3/4-0.003	77
Aluminium	ACG 1 - 0.003	92
Carbon fibre	ACG 3/4-0.003	10.1
Carbon fibre	ACG 1 - 0.003	9.6

The difference in the sagitta for the various types of honeycomb material is mainly due to their different heat conduction coefficients. The difference from aluminium to carbon fibre skin is due to the smaller thermal expansion coefficient of the carbon fibres, attenuated by its smaller heat conduction coefficient. The deformations are considerably decreased by the fact that the bi-cells are mechanically disconnected from the support structure but are acting as an efficient heat screen.

The thermal behaviour of the proposed carbon fibre support structure has not yet been analysed, but the deformations are expected to be even lower than in the above-mentioned case of the mono-block carbon fibre version since in this open structure the convection of air will tend to equalise the temperature difference.

7. Test Results

7.1 Experimental set-up

A 4.3m long, 1.7m wide carbon fibre prototype, instrumented with nine bi-cells, 4.3m long, has been exposed to the parasitic μ beam of the EHN2 hall. The bi-cells have been mounted in 3 groups with distances of 0.8 m to cover the whole width of the support. The configuration of the instrumented prototype reproduces the configuration foreseen for the ATLAS μ-detector based on the Jet Cell Chambers. In addition, data have also been taken with two chambers, not mounted on the C-fibre support, put on the beam one behind the other, either with the wire plane parallel to the beam or at an angle.

The main performance characteristics are determined by a preliminary analysis of the test beam data.

While the results show that the performances required in the ATLAS μ-detector design are already achieved, there is room for improvement by means of more refined analyses, optimisations, and future hardware improvements (e.g. operating the Jet Cells at higher gas gain or optimised readout electronics).

In the following, the test beam results concerning the three most relevant aspects of a μ-tracking detector are reported. They are:

- The single wire intrinsic resolution
- The multi-track capability
- The control of the systematics.

The test beam set-up is shown in Fig. 13. The module prototype consists of 9 bi-cells 4.3m long, mounted on a high-precision C-fibre support, 4.3 m x 1.7 m. The support is held steadily on iron feet. The beam is defined at the trigger level by the two large scintillation hodoscopes and a small scintillation counter. The position of the particles in the direction of the wires is measured by a plane of RPC counters, with 3 cm strips oriented vertically located upstreams. Finally two sets of high pressure drift tubes ("flowers") provide two precision external reference systems. They are fixed on glass supports with low thermal dilatation.

7.2 Chamber operating conditions

The chambers are operated with an Ar/Ethane 65/35 mixture at atmospheric pressure. No record has been taken of ambient pressure and temperature. Therefore no corrections for pressure and temperature changes have been applied. The HV settings were in the range of 4 kV for the sense wires and 3 kV for the potential wires. A large plateau with efficiency above 99% is shown by a HV scan.

The wire signals are read using the preamplifier-shaping amplifier-discriminator chain used on the HELIOS chambers. The time is measured with the 1ns bin LeCroy 2277 multihit TDCs.

7.3 Single wire intrinsic resolution

The intrinsic single wire resolution is shown as a function of the drift distance in Fig. 14; the global distribution, averaged over the full drift distance, for two different wires is shown in Fig. 15. The single wire resolution has been determined by the distributions of the quantity

$$S = Y_2 - (Y_1 + Y_3) / 2 ,$$

where Y_1, Y_2, and Y_3 are the distances from the wires of the track points measured by three consecutive wires. The single wire resolution, σ_{SW}, is obtained from σ_S , by the relation

$$\sigma_{SW} = \sqrt{2}/3 \times \sigma_S .$$

Finally, in Fig. 16, we show the distribution of the residuals from the fit of 8 point tracks. The gaussian fit gives a σ = 140 μm. Note that no corrections were applied to this determination.

From Fig. 14 and Fig. 15, the resolution is found to be 145 μm, averaged over the complete drift region.

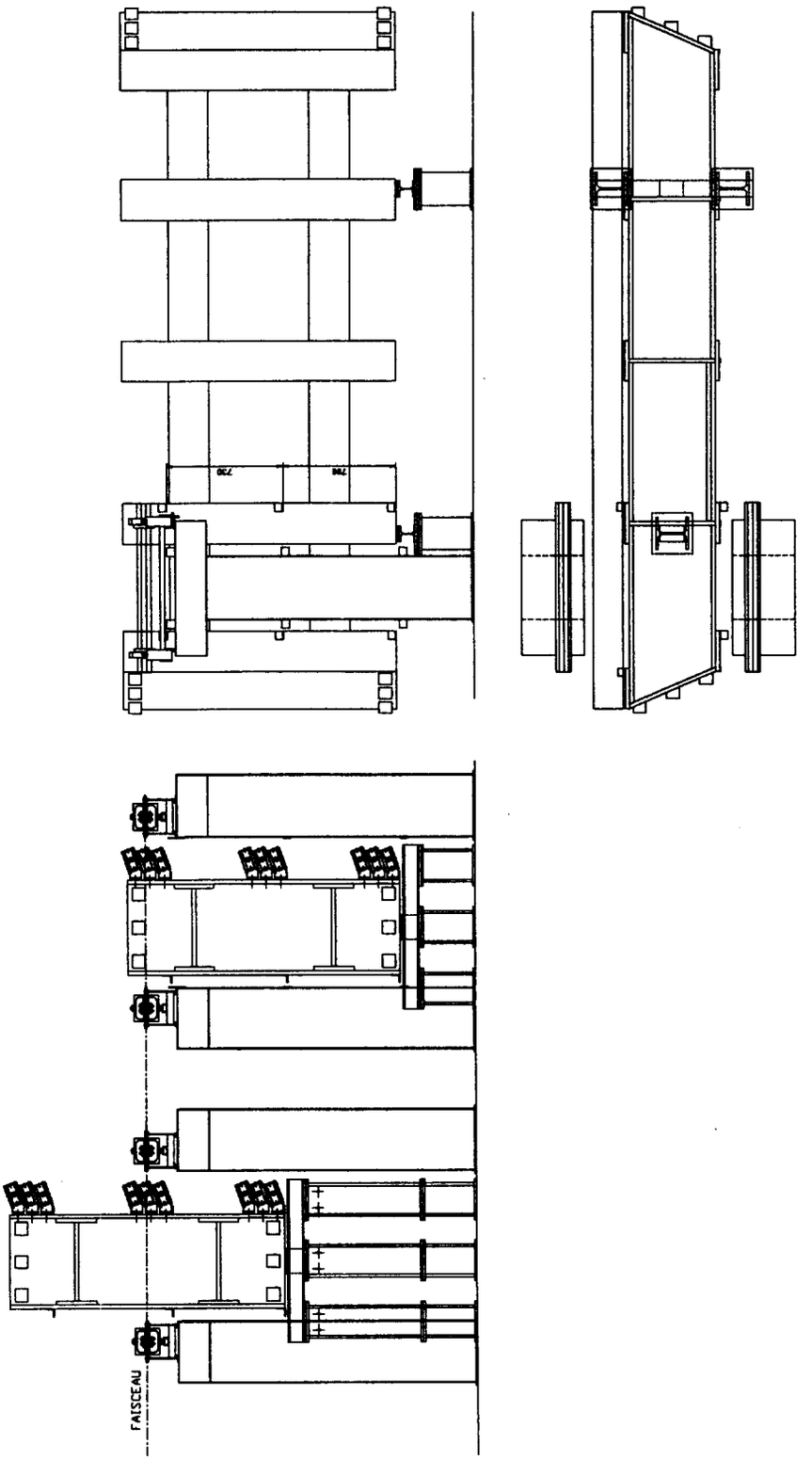

Figure 13
Layout of the Jet Cell Test area. The prototype was measured in two positions, with the Dubna 'flowers' providing the external reference, located before and after the Jet Cell prototype

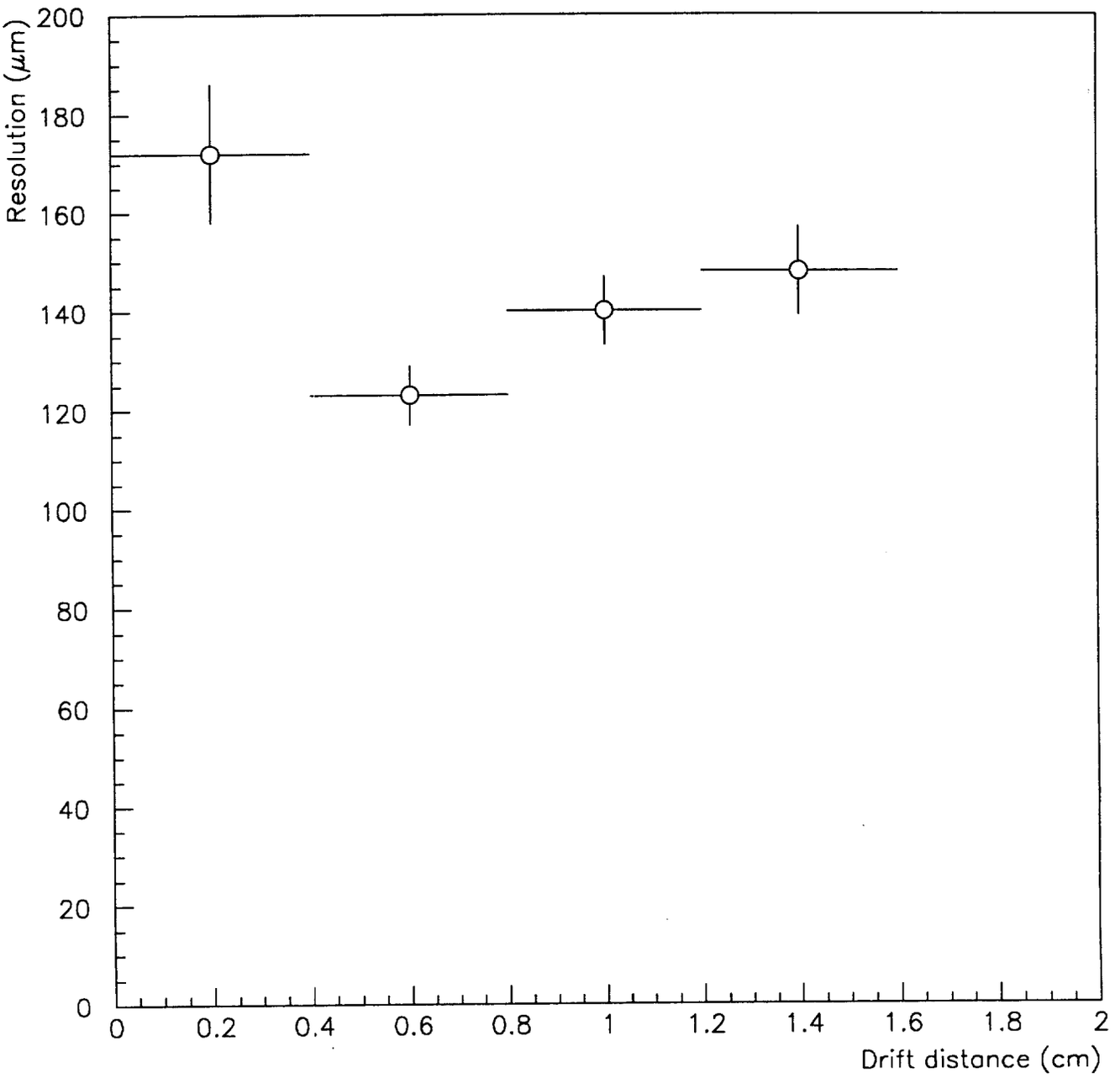

Figure 14
Single wire resolution versus drift distance.

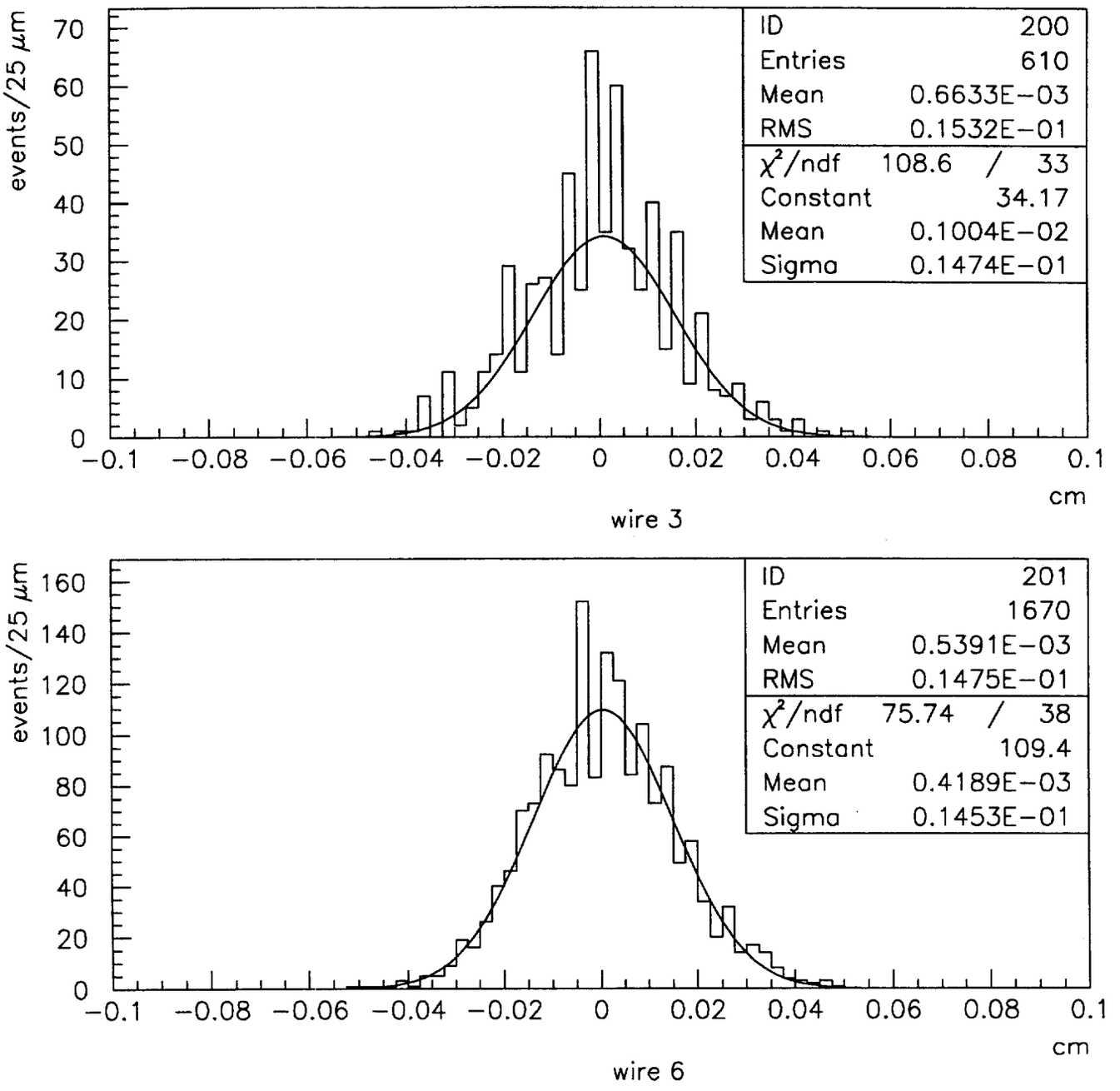

Figure 15
Resolution for two different wires, averaged over the full drift region.

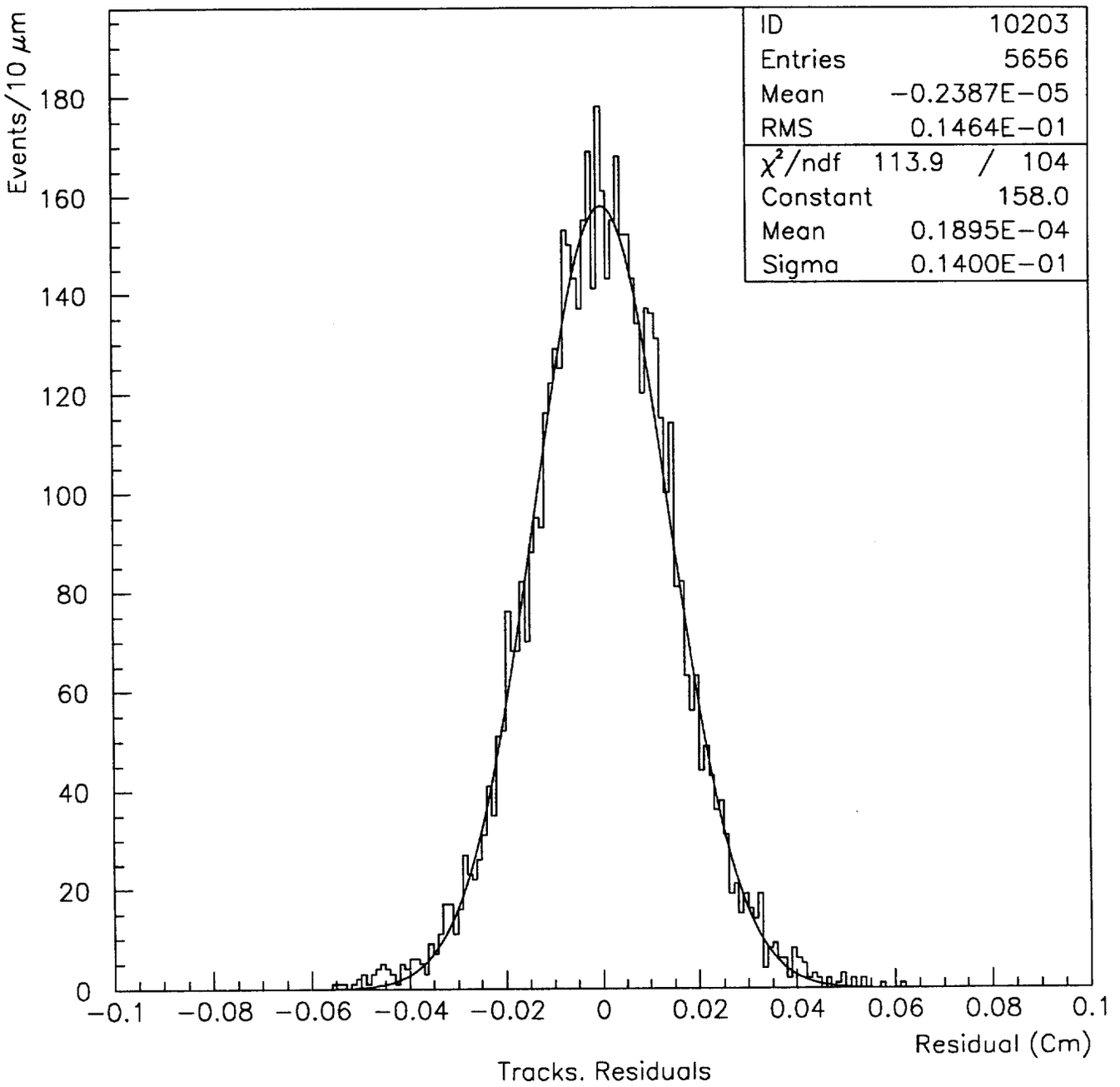

Figure 16
Distribution of residuals from a track segment fit to eight measurements.

7.4 Single wire intrinsic resolution: expected

The test beam results presented in the previous section were not taken under optimum conditions. During the tests, emphasis was placed on understanding systematic effects (section 7.6) and on a general understanding of the operating parameter space. Most importantly, we decided for economy of time and financial resources to reuse a rather old electronic readout system, which was optimised for a slow gas and employed very fast shaping for very good two-track resolution.

However, in the JC-technology, the single wire resolution enters in a significant way into the total error budget. It is therefore instructive to analyse the achievable resolution, as measured e.g. by other groups under comparable conditions of drift geometry and drift gas. We insist here once more that the results quoted are valid for the use of a 'fast', saturated drift gas, as was explained in Section 1 and as will be used in the ATLAS spectrometer.

The Zeus Forward Tracker [5] is a 'Jet Cell' tracker with 6 sense wires in a cell and a maximum drift distance of ± 12 mm. Using the published values for the resolution obtained with a gas of Ar/C_2H_6 (50:50) one estimates extrapolating the measurements for 12 mm to 20 mm and averaging the full drift cell of:

$$\sigma(\text{ZEUS, Jet Cell}) \leq 125\mu m$$

We have also exposed a one metre prototype with tilted Jet Cells to cosmic ray muons and have observed a resolution, again averaged over a ± 20 mm drift distance of $\sigma = 130\mu m$. This value is an 'on-line' resolution, without further corrections, and using non-optimised electronics. We conclude that in our good drift geometry using optimised electronics, a resolution of

$$\sigma \approx 120\mu m$$

is achievable, judging by our own test results and those of other groups. It should also be noted that drift in jet cell geometry at saturated velocity results fundamentally in a better resolution compared to drift in the same gas but at electric fields E too low to achieve saturation. This is due to the fact that at such low fields the longitudinal diffusion increases. As a consequence, a cylindrical drift geometry cannot give a better resolution than a 'jet cell' geometry for the same gas conditions at comparable maximum drift distances.

7.5 Multi-track capability

The background radiation at LHC, the showering of high energy μ in the matter, and the δ-rays will be the origin of additional tracks or hits accompanying the μ-track.

If the technique used for μ detection only allows for the detection of the first hit, some points of the μ track will be lost, with a reduced performance in pattern recognition and momentum resolution. Variations of the background level with respect to the present expectations, which are only known with large uncertainty, can strongly affect the μ detection. A technique which provides multi-track detection capability, is, therefore, more robust. The Jet Cell chambers, adopted in many detectors, have been already shown to allow to reconstruct tracks with 2-3 mm separation.

The two track separation has been measured for our bi-cells with the test beam data. Events with two tracks detected in one bi-tube and confirmed in a second bi-tube, placed behind the first one on the beam, are selected.

The track separation is plotted in Fig. 17. The separation between the pair of hits of the two tracks is plotted in Fig. 18. The figures show that if the separation is above about 2.5 mm, two tracks in the same cell are reconstructed. This is nicely illustrated in Fig. 19, where the display of one event is shown. Two tracks, slightly convergent, can be seen in the plot. Two independent hits are reconstructed for hit separations larger than approximately 2.5 mm.

7.6 The control of systematics

The stochastic resolution of a superlayer is reduced compared to the single wire resolution by the factor $1/\sqrt{n}$, where n is the number of wires hit per superlayer. In the central superlayer of the sagitta measurement configuration, the number of wires could also be increased, in order to further improve the resolution.

In the actual detector such precisions are realistically achievable only if the systematics are controlled below that level, which will be the principal challenge for the ATLAS muon detector.

We have made a test of our prototype in the ENH 2 μ beam, in order to establish the level of control of systematics with particles measured in the chambers . For this purpose the prototype has been exposed to the beam in the position 1 shown in Fig.13; subsequently, it has been raised by 73 cm into position 2. The external reference was provided by the two 'flower' reference systems.

The data have been analysed as follows: in both positions the height X_i of the illuminated sense wires has been measured in the coordinate system of the flowers. Therefore the height X at which the track crosses the vertical plane containing a wire of the JC chambers has been calculated using the flower measurements and then plotted versus the raw TDC time measured on that wire of the JCC (see Fig. 20). The two parts of the plot, with positive and negative slope, correspond to tracks traversing the cell on the two sides of the wire. The wire position is given by the value of X at which the change in slope takes place. This can be determined as the crossing point of the straight line fits to the two parts. The measurements of two sets of 4 wires, before and after the displacement has been analysed, together with the difference which represent the displacement of corresponding wires in the reference system before and after the shift of the module.

The average displacement for the 4 subsequent sense wires is

$$\Delta X_{mean} = \frac{1}{4}\sum_{i=1}^{4}\left(X_{i,a} - X_{i,b}\right) = 280(22)\mu m,$$

where a and b stand for the measurements after and before the lift. This displacement has to be compared with the difference of the total shift of the module as measured with direct optical levelling

$$H_{lift} = 730.573(35) \text{ mm}$$

and the distance between the wires as expected from the construction

$$D_{wire} = 730.223\ (43) \text{ mm}$$

This value has been corrected for the slightly different inclinations of the support structure during both measurements.

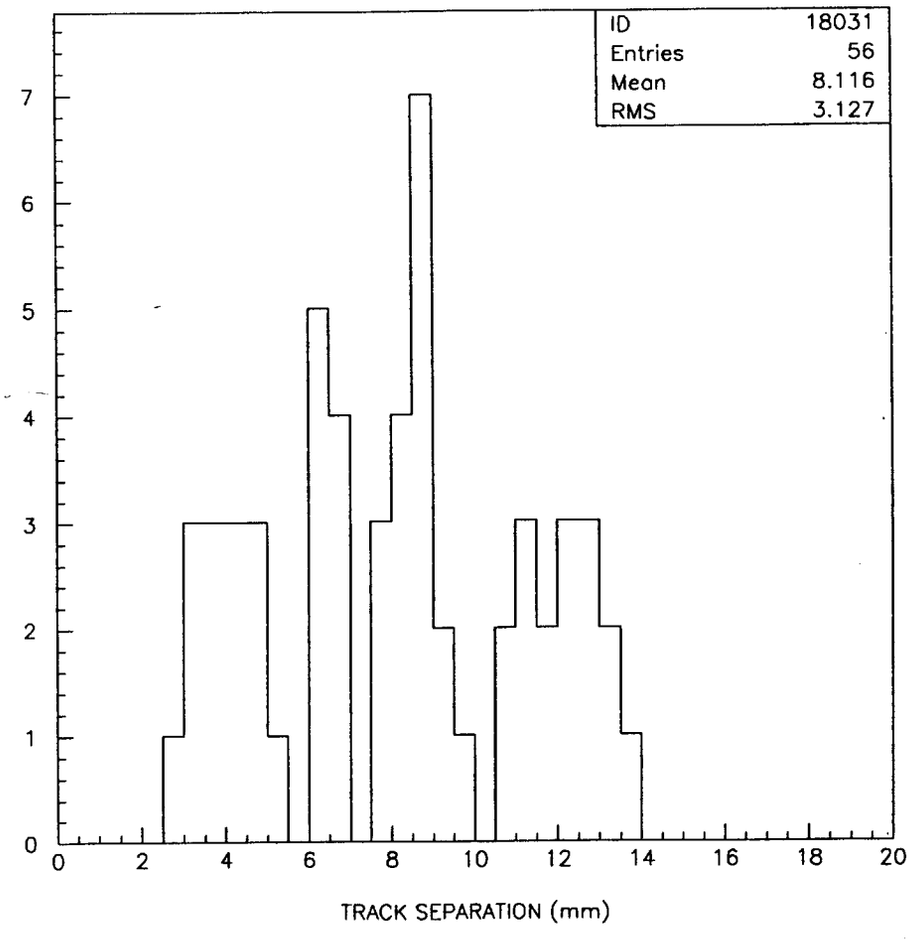

Figure 17
Track separation for two-track events measured in the Jet Cells, showing a two-track resolution of approximately 2.5 mm.

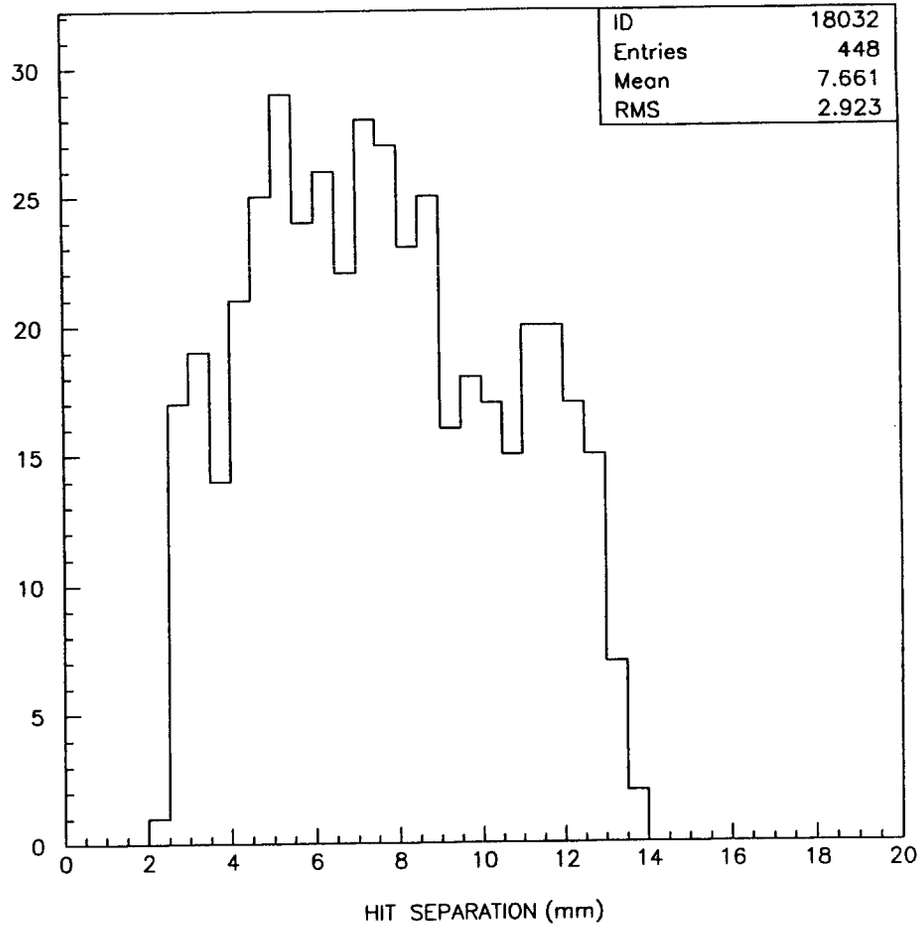

Figure 18
Two-hit separation recorded for the sample of two-track events displayed in Fig. 17

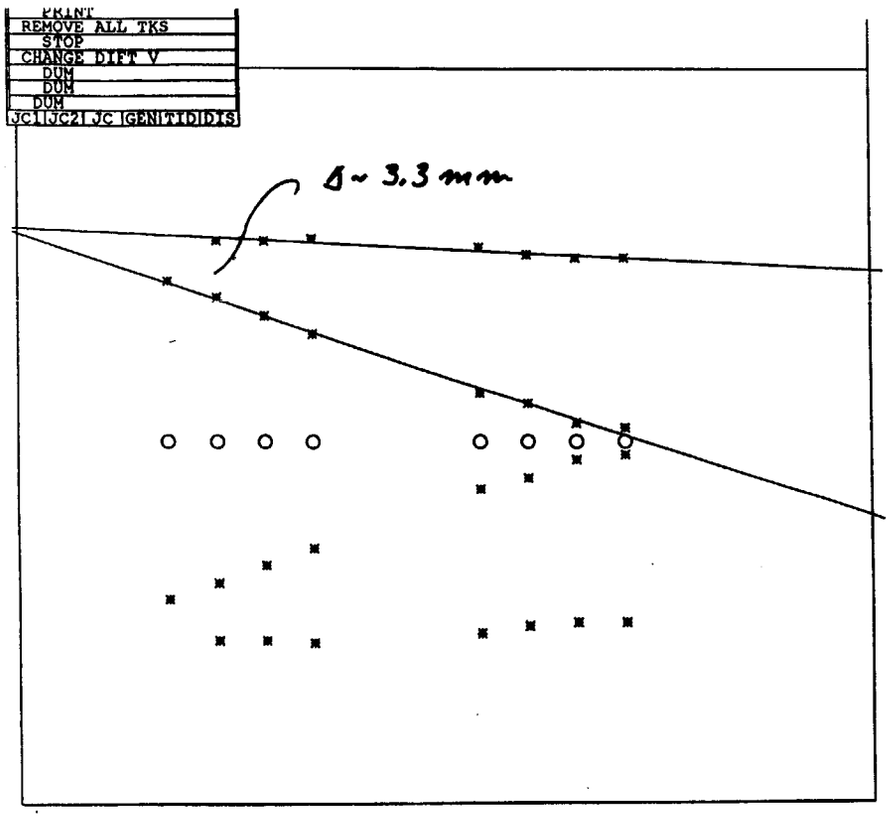

Figure 19
Event display of a two-track event as measured in one Jet Cell.

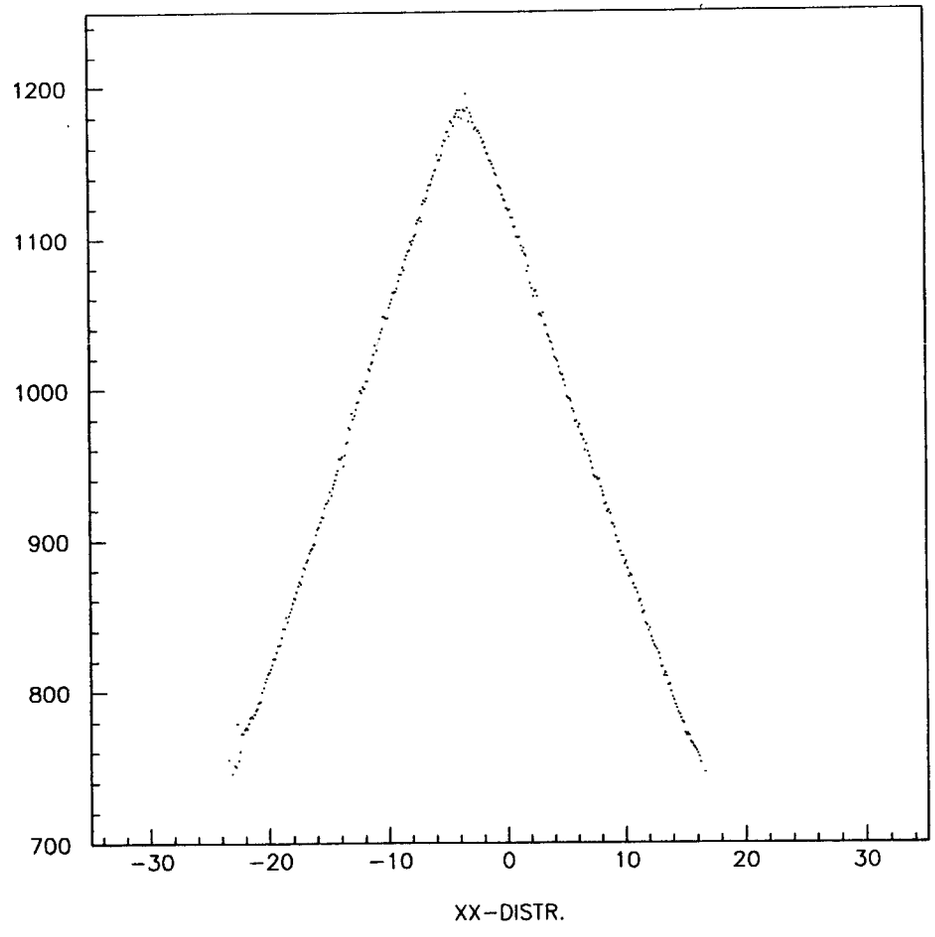

Figure 20
The reference position, measured in the 'flowers', versus raw TDC time measured for a Jet Cell wire. The crossing of the right and left distributions determines the position of the wire in the Jet Cell.

A small change in the flower position during the two measurements produces a small correction

$$\Delta_{flower} = 11(20)\mu m$$

As a (still preliminary) result we get

$$D_{wire} + \Delta X_{mean} - H_{lift} + \Delta_{mean} = -59\ (63)\ \mu m$$

This result shows that the systematic errors of the Jet Cell set-up have now been controlled to a level consistent with the analysis of Chapter 5.

8. A Comment on Costs

In the following, the costing tables based on information presented to the CORE committee are included. The prices have been somewhat updated and show consistent numbers for the different technologies for common items like electronics, alignment and common installations (e.g. gas systems).

The prices for the carbon fibre support structures may appear high and a comment should be made. One indication is for a totally industry-made product, delivered to CERN. It is estimated based on the purchase of the prototype support and linearly extrapolated to the final system. If, however, this item were to be manufactured in one of the collaborating institutes, the purchase of the raw material (carbon fibre sandwich plates, brackets, glue, etc.), the assembly tools and the rental of a large precision drill would lead to an economy of 6.3 MSFR in the material budget. The 5 years of production would, however, imply another 45 men years of skilled men power.

The estimate of the manpower needed is based on experience of typical production rates achieved during the construction of large scale detectors like the Barrel RICH in DELPHI or the central trackers in R807 and UA1. While we will use automated production methods, as described previously, our manpower estimate is not affected significantly. We have learned from past experience that automation results in better quality control but has only a modest impact on the overall construction time.

Table 3: Comparison of the cost for the canonical and optimised layout (prices in KCHF)

	JCC canonical [ATLAS]	JCC optimised layout [Figs. 2 and 3]
Chamber + support	8800*	8015*
Production facilities	880	670
Price/m2 (5000m2)	3	3
Production facilities	4	3
Test	150	150
Fixtures & ext. supports	1144	752
Orientable support	150	100
Total mechanics	**11131**	**9693**
Number of Readout channels	190368	129824
Barrel	132384	65920
Small chambers		23680**
Endcap	57984	57984
Total electronics cost/channel	18	18
Total electronics	**3427**	**2337**
HV system	**600**	**600**
Gas system	**1000**	**1000**
Alignment system	**800**	**800**
Installation tools	**1000**	**600**
Monitoring/slow control	**1200**	**1200**
GRAND TOTAL	**19176**	**16248**

* This price estimate includes the materials and the fabrication tools. If the C-fibre support structure were completely built by industry, it would result in additional costs of 6.3 MCHF (optimised layout) and 7.1 MCHF (canonical layout).

** In the estimation for the electronics cost the channels of the small chambers have been multiplexed by 4.

Acknowledgements

The work described in this note was carried out to a large extent during the past nine months. We are grateful to many colleagues in ATLAS who have shared their experience and knowledge with us. We gratefully acknowledge the financial and technical support made available to us by the Directors and Department Heads of the Collaborating Institutes. Finally, we enjoyed the friendly and constructive atmosphere we shared with the HPDT group in our common test beam area.

References

[1] J.C. Chevalley, Jet Cell group: Internal Note (Nov. 1990).
[2] W. Blum, High-precision drift tubes MPI-PhE 93-12 (June 1993).
[3] J.C. Gayde and C. Lasseur, Jet Cell Chambers: Dimensions et Déformation d'un Prototype de Support, ATLAS Internal Note (Aug. 1993).
[4] W. Richter: Temperature problems of muon chambers; Internal note to the ATLAS Muon group, Dec. 1992.
[5] M. Herzog, Experimentelle Untersuchungen an der planaren Driftkammer FTD2 des ZEUS-Vorwärtsdetektors. BONN-IR-92-50 (1992).

Appendix 1

PARAMETER LIST

ATLAS MUON JET CELL CHAMBER SYSTEM

1) SINGLE CELL PARAMETERS

single wire resolution [μm]	150	measured
two-track resolution [μm]	2500	based on measurements
second-coordinate capability ?	in principle, yes	
If yes, resolution	$\sigma \approx 3$ cm	
gas mixture	candidates: $He/CF_4/C_4H_{10}/CO_2(85/5/5/5)$ or $N_2/CF_4/CO_2/CH_4(80/6/4/10)$	
v_D at operating voltage (or range of v_D)	4 cm/μs	
t_D max.	500 ns	
θ (Lorentz)	< 12° at 0.9 T	
dv_D / d Pressure	1.5×10^{-4} per 1 mm Hg	
dv_D / d Temperature	3.5×10^{-4} per 1° K	
total amount of flammable gas [kg]	probably: zero	
gas gain	$\leq 10^5$	
max. high voltage	5 kV	
wire material	Cu-Be; preferred also for sense wires	
wire diameter	~ 40 μm for sense wires 100 μm for potential wires	
wire tension [g]; [% of elastic limit]	≤ 30%	
wire sag	40 μm max.	
method of wire location	injection moulded plates or combs	
neutron sensitivity	2×10^{-3} (no energy threshold)	
γ sensitivity	2×10^{-2} (no energy threshold)	
insensitive zone at chamber ends (plugs) [up to external cover] [cm]	1 cm ≤ 4 cm	

2) SUPERLAYER PROPERTIES

relative precision between wires	< 20 μm	measured
flatness of supports	< 1 mm	based on measurements
precision of wires relative to alignment references	20 mm	
procedures for aligning wires relative to alignment references	by precision mechanical construction	
number of sense wires on common HV line	not yet specified	
uniformity of gas volume	most open structure of the three technologies	
thermal stability of support: transverse; in plane;	} 10^{-6} /°C	
weight of chamber + support / m^2	≤ 18 kg / m^2	
radiation length of chamber + support	4% Xo	
average resolution per superlayer	61 μm	

3) CONSTRUCTION FEATURES

total number of channels	190368/129824	
number of modules to be installed	512 large scale and 128 small	
number of alignment lines	?	
type of alignment lines (3-points; 4-points ...)	3-point Rasnik	
number of gas connections	2 per bi-tube (16 wires)	
verification of superlayer precision	by photogrammetry	
% of value added by ATLAS Institutes, added by Industry	?	
mechanical rigidity of super module :	≤ 1 mm max. sagitta (8 m long chamber)	
largest super module: fabricated to date	4.3 x 1.7 m^2	
required for ATLAS	≤8 x 3 m^2	
experience with technology in previous experiments.	Jet cells is the most frequently used drift chamber technology	

Appendix 2

Wednesday, 1 September 1993

MEMORANDUM

To/A: ATLAS Muon Panel

cc:

From/De: Jet Cell Group (B.Goret, W.Klempt)

Subject/Objet: Influence of the gravitational deformation to the Sagitta Measurement

---

This note summarises the calculation performed to understand the influence of the gravitational deformation of the carbon fibre modules in the ATLAS muon spectrometer on the error in the saggitta measurement.

To estimate the elastic deformation of a super module caused by its own weight and the weight of the jet cells, we assume first, that the modules can be described as uniform plate kept in position at 4 supporting points (fig. 1).

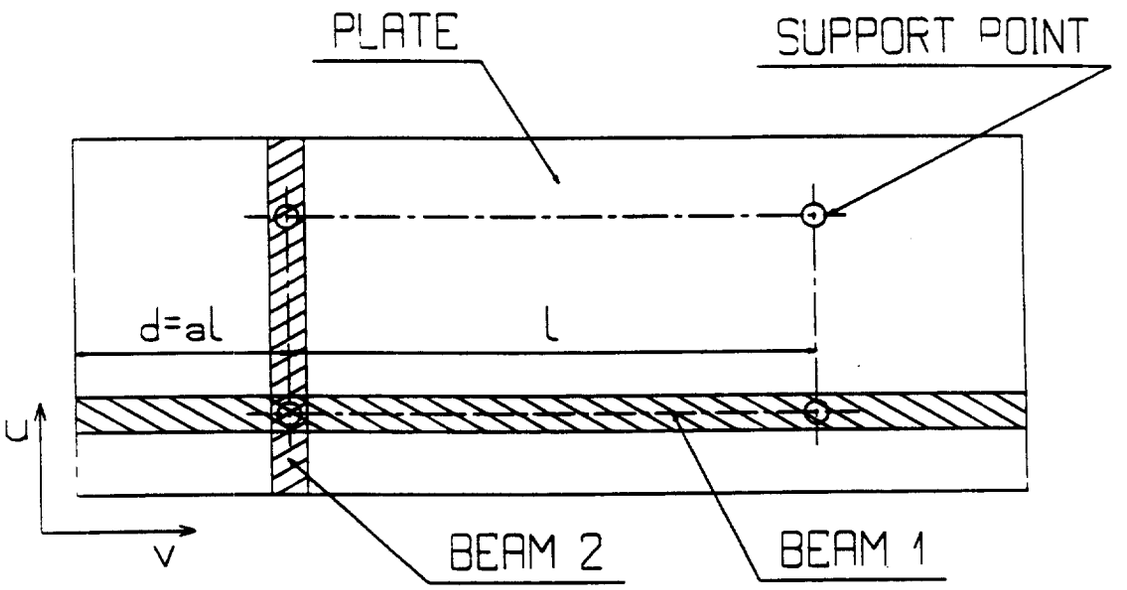

Fig. 1 Plate representing a super module

Finite element calculations have shown that the deformations of a super module in the outer layer (length ≈ 9m) can be kept to the order ≈1mm. Therefore we describe the mechanical behaviour of this plate by 2 uniform beams, perpendicular to each other, each of which supported on 2 points. Then the deformation somewhere in the plate y(u,v) can be estimated in first order to

$$y(u,v) = y_{Beam1}(v) + y_{Beam2}(u).$$

Classical engineering gives us the deformation on an uniform beam

$$y(x) = (1/E*I) * \iiint q(x)\, dx^4$$

Where x runs along the beam, E is the Young's module, I the moment of inertia, and q is the mechanical load per unit length. Since q is constant over x , the deformation can be described by polynoms of the 4^{th} degree. The integration constants are determined by the various boundary conditions of the problem.

The position of the supporting points have been determined by the condition, that the deformation at the extremes and the middle point of the beam should be equal. In this way the average deformation over the whole beam is minimised. Let l be the distance between the supports and d=a*l be the distance between an extreme and the near support. Then the equality of the maximum deformations lead to

$$a = 0.403$$

which gives the relative position of the supports.

In ATLAS the muon spectrometer is composed by 3 layers of super modules at radii R_1, R_2, R_3 with widths B_1, B_2, B_3 and length L_{11}, L_{12}, ... ,L_{33} as schematically indicated in fig 2.

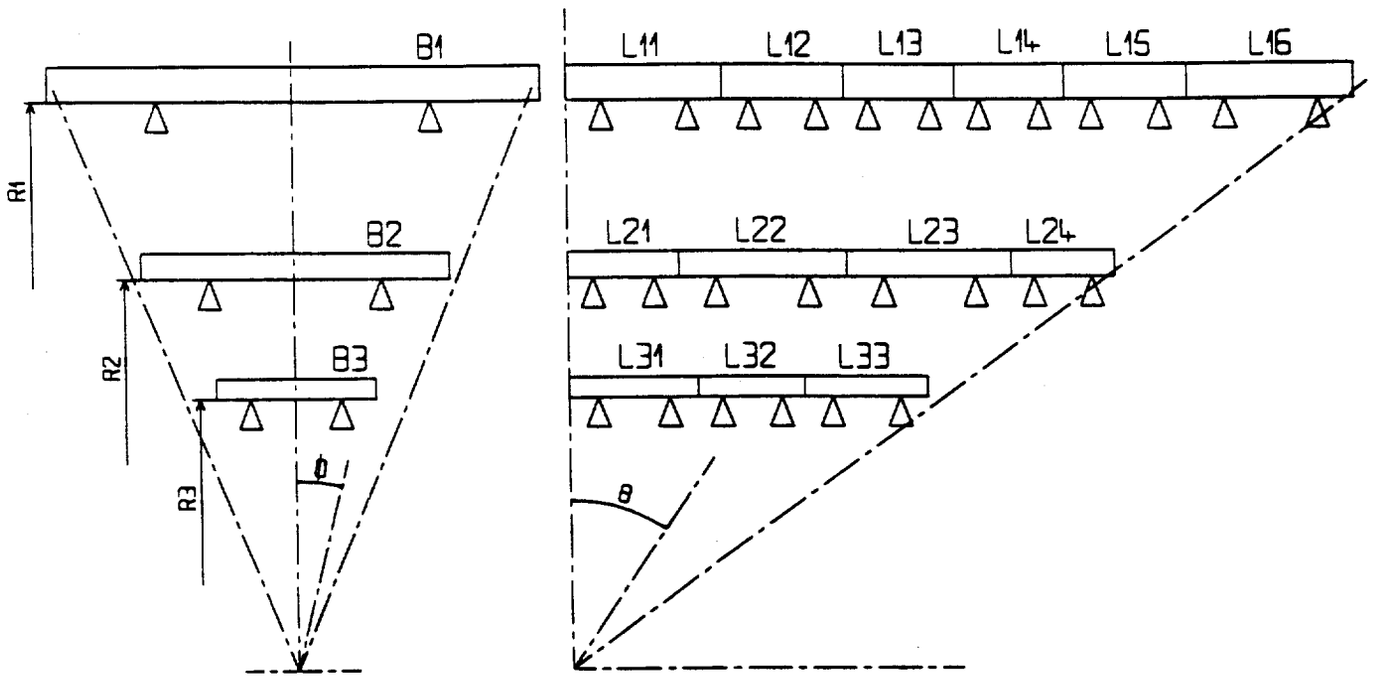

Fig.2 Schematical layout of the muon chambers in ATLAS

To evaluate the error on the saggitta due to the deformation of the different modules, we normalise the maximum deformation of the modules of the different layers 1,2,3 to be

$$ymax_{B_i} = 1 \text{ mm}, i = 1,2,3$$

in the direction ϕ. The maximum deformation in direction θ are then given by

$$ymax_{L_{i,j}} = ymax_{B_i} * (L_{i,j}/B_i)^4$$

The saggitta of a muon track is given by

$$S = x_2 - x_1 * (R_2-R_3)/(R_1-R_3) - x_3 * (R_1-R_2)/(R_1-R_3)$$

where x_i is the position of the track in the layer i. When the deformation is known with a relative accuracy of α%, the error on the saggitta due to the deformation in the layer is given by

$$\sigma S_i(x_i) = \alpha * C_i * y(x_i) * (x_i/R_i)$$

$y(x_i)$ is the deformation at x_i,C_i is the corresponding coefficient of x_i in the saggitta formula, and x_i/R_i accounts for the angle of impact of the track.

We assumed in our calculation

$$\alpha = 10\%$$

In the following we give the respective values for $L_{i,j}$, B_i and R_i used in our calculations.

$L_{i,j}$[mm]	j=1	2	3	4	5	6
i=1	2670	2080	1920	1920	2130	2950
2	1900	2870	2870	1800		
3	2220	1820	2100			

$B_1 = 8560$mm, $B_2 = 5350$mm, $B_3 = 2760$mm

$R_1 = 9825$mm, $R_2 = 6770$mm, $R_3 = 4686$mm

For each module we have now calculated the corresponding mean error contribution to the saggitta $\sigma S_{i,j}$ listed below

$\sigma S_{i,j}$[μm]	j=1	2	3	4	5	6
i=1	2	9	15	20	22	17
2	4	11	20	44		
3	7	11	26			

This yields in a mean error for each layer

$$\sigma S_i = (\Sigma \sigma S_{i,j} / \Sigma L_{i,j})$$

$$\sigma S_1 = 13\mu m, \sigma S_2 = 18\mu m, \sigma S_3 = 15\mu m$$

The total error contribution to the saggitta is the given by

$$\sigma S = \Sigma \sigma S_i = 46\mu m$$

Up to now we have only considered modules at $\phi=0^\circ$ or 180° . Averaging over all module angles gives

$$\sigma S_W = \sigma S * (1 + 2 \cos 45^\circ)/4 = 28\mu m$$

Appendix 3

Jean Christophe GAYDE CERN / AT-SU
Christian LASSEUR CERN / AT-SU
Julian NORTON CERN / AT-SU

November 12th, 1993

CLOSE-RANGE PHOTOGRAMMETRY

The aim of close-range photogrammetry is to provide a quick and precise 3D measurements system. The size of the object measured can vary from just a few centimetres to tens of metres. This method was used to measure the dimensions and deformations of the prototype support of the Jet Cell, and was seen to be efficient.

Concept

Photogrammetry produces 3D coordinates of reference points using a series of photos.

The photos are taken using a 'metric camera', such that:

- each target points appears as an image point on many photos;
- each photo contains the image of many target points.

Basically, the 3D coordinates of the reference points on the target object can be found from:

- the coordinates of the reference point images on the photos;
- the characteristics of the camera (position, orientation, focal length, etc.).

The imaginary line in space between each image point and the centre of perspective of the camera extends to form a line on which the target point lies. The intersection of two or more of these lines will define the target point in 3D space.

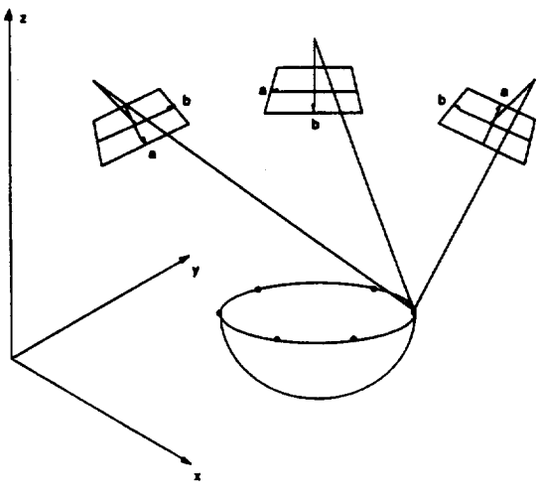

In photogrammetry, the convergent geometry described above is calculated using a method known as 'bundle adjustment'. This determines at the same time the parameters of the camera and the coordinates of the target points. The basic principles behind a bundle adjustment are as follows:

- each target point has a 'bundle' of perspective rays, where a ray is the line between the target point and the image point via the perspective centre of the camera;
- the geometry within the bundle is considered fixed;
- all homologous rays (the rays going to the same target point) intersect at the same point.

The calculation is done using the least squares method, in order to have a solution which satisfies the bundle adjustment conditions described above.

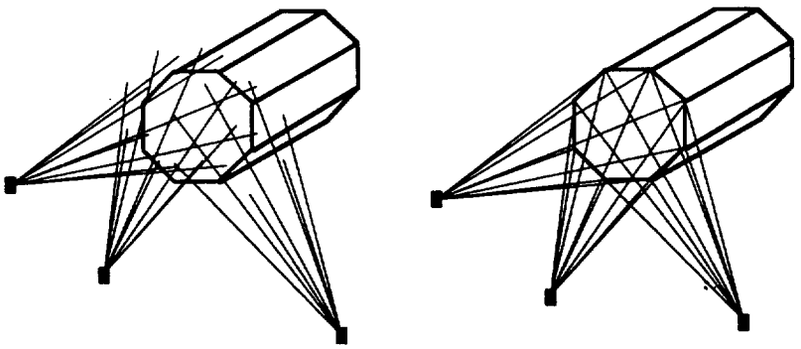

Notes:

As with all systems of angular measurement, a scale factor is necessary to calculate the 3D coordinates of the target points. This factor is obtained by measuring very accurately the distance between some points on the object. This is usually done by using one or more invar scale bar placed on or near the target object so that they appear on the photos.

The cameras used are metric cameras with variable format and focal length combinations. The choice of these two parameters depends on the configuration of the objects to be measured and the accuracy required. Examples of cameras: format 24x24 cm with focal length 160 mm or 240 mm; format 12x12 cm with focal length 120 mm; etc.

The image coordinates are measured automatically, with a precision of 0.2 to 0.3 μm. This is done using a monocomparator equipped with a CCD camera.

The accuracy of the System

Close-range photogrammetry can produce very accurate results when performed under optimum conditions (this optimisation is found by simulation).

The following formulas give an estimation of the absolute precision.

$$\sigma_{coord} = q \times S \times \sigma_{mono}$$

or again:

$$\sigma_{coord} = q \times d \times \sigma_{angl}$$

where:

S = photo scale

σ_{mono} = accuracy of image coord measurement using monocomparator (~ 0.2 or 0.3 µm)

q = factor depending on the geometrical configuration and the redundancy in the measurements (~ 2 or 3)

$\sigma_{angl} = \sigma_{mono}$ / focal length

d = average distance from camera to object

Jet Cell Support: q = 2.5, d = 3 m, σ_{mono} = 0.3 µm, focal length = 120 mm → σ_{coord} = 19 µm

Results Obtained from the Measurement of the Jet Cell Support Prototype (vertical position)

The vertical position corresponds to the least favourable suspended position in terms of precision. The coordinates are such that: X = length, Y = breadth, Z = width.

- Typical average standard deviations: s_X= 15 µm, s_Y= 36 µm, s_Z= 15 µm;
- Selection of results:

Point	X (mm)	Y (mm)	Z (mm)	sX (mm)	sY (mm)	sZ (mm)
OC12	0.027	-316.788	-371.911	0.011	0.022	0.010
OC13	0.120	-316.839	-610.944	0.011	0.022	0.011
OC14	0.149	-316.878	-700.161	0.011	0.022	0.011
OC15	0.121	-316.916	-789.334	0.011	0.022	0.011
OD1	999.917	-316.271	819.146	0.012	0.028	0.013
OD2	999.924	-316.345	729.911	0.012	0.028	0.013

Note: The systematic errors are eliminated by following certain measurement techniques (e.g. rotating the camera by 180 degrees).

Some advantages

Other than the precision gained by photogrammetry, there are a number of other advantages:

- data capture is quick, and therefore improves accuracy. 30 minutes was sufficient to take 20 photos of one position, which was enough to cover all the surface of the prototype Jet Cell support;
- the number of photos required is not dependant on the number of targets on the object, but the surface area of the object;
- with close-range photogrammetry it is not necessary for the target points to be fixed and stable, this is just the case with the classical method;
- the coordinates system used is free and can be defined by the target object (as in the case of the Jet Cell), or externally, if some of the target points are known in such a system;
- dynamic measurements are possible: when the object is moving, the cameras can be fixed and a series of photos taken of a moving object;
- photogrammetric measurements can be treated simultaneously with other types of observation (e.g.: distances, angular measurements by theodolite, etc.).

The future

Videogrammetry, using CCD cameras, gives good results with small target objects. The digital image allows an 'on-line' photogrammetric system to be envisaged. The major problem is the small field of vision of each photo.

Dimensional calibration of the Jet Cell Chambers

In order to take account of the shape and dimension of the Jet Cell chambers when analysing the particle tracks, the following calibration method is suggested. This method is based on the rigidity of the supports, and the fact that they maintain the same shape in the same position. Basically, this involves measuring directly on the bi-tubes under experimental conditions.

For this purpose:

- the chambers should be equipped with:
  - two reference points placed on the top of each wire support plate of the bi-tubes;
  - some other points, distributed on important places (e.g.: the system of alignment supports);
- this will provide between 25 to 30 points per m^2 of chamber, so giving between 150,000 to 200,000 points for the 5000 m^2 muon detector;
- an appropriate scale system should be designed and then fixed on each chamber, in order to obtain maximum precision;

- for the calibration, the chambers must be placed in the same position and conditions that they will have in the experimental zone;
- the calibration zone must be optimised for photogrammetric work.

Data capture is very fast, so many chambers can be photographed in one session. This minimises the downtime for surveying during the construction of the experiment.

Once in the experiment, the measurement of just some points will allow the reconstruction of the position of all the other points.

Other uses for close-range photogrammetry

Close-range photogrammetry can be used to measure all sorts of objects. It can be used on all kinds of muon chambers as well as on all types of detectors. The application areas can be, for example:

- the calibration of many detectors (or pieces of detector) at the same time;
- dimensional control;
- shape control, where the surface can be reconstructed using a dense pattern of points on the target object;
- the measurement of spatial positions (mounting control, relative position of detectors);
- dynamic measurements of moving objects.

Conclusion

Close-range photogrammetry seems to be the most elegant and adaptable system for the metrology of physics experiments, because of:

- the precision;
- the speed;
- the ease of use.

Because it is easy to determine a great number of points with little effort, large databases of 3D coordinates can be built for all the detectors in the experiment.

It should also be remembered that traditional, stereo-photogrammetry can play an important role in less-precise applications (a few mm). It is not necessary to place targets points on the object, and is also suited to preparing metrology in experimental zones that require surveying (e.g.: position of supports, rails, etc.).